Bioinspiration & Biomimetics

TOPICAL REVIEW

Aerodynamic efficiency of gliding birds vs comparable UAVs: a review

Bioinspiration & Biomimetics

TOPICAL REVIEW

Aerodynamic efficiency of gliding birds vs comparable UAVs: a review

Christina Harvey* and Daniel J Inman

Department of Aerospace Engineering, University of Michigan, Ann Arbor, United States of America
* Author to whom any correspondence should be addressed.

E-mail: harveyca@umich.edu

RECEIVED
23 July 2020

REVISED
22 October 2020

ACCEPTED FOR PUBLICATION
6 November 2020

PUBLISHED
19 April 2021

Keywords: bird gliding flight, avian aerodynamic efficiency, bioinspired UAV, low Reynolds number

Supplementary material for this article is available online

Abstract

Here, we reviewed published aerodynamic efficiencies of gliding birds and similar sized unmanned aerial vehicles (UAVs) motivated by a fundamental question: are gliding birds more efficient than comparable UAVs? Despite a multitude of studies that have quantified the aerodynamic efficiency of gliding birds, there is no comprehensive summary of these results. This lack of consolidated information inhibits a true comparison between birds and UAVs. Such a comparison is complicated by variable uncertainty levels between the different techniques used to predict avian efficiency. To support our comparative approach, we began by surveying theoretical and experimental estimates of avian aerodynamic efficiency and investigating the uncertainty associated with each estimation method. We found that the methodology used by a study affects the estimated efficiency and can lead to incongruent conclusions on gliding bird aerodynamic efficiency. Our survey showed that studies on live birds gliding in wind tunnels provide a reliable minimum estimate of a birds' aerodynamic efficiency while simultaneously quantifying the wing configurations used in flight. Next, we surveyed the aeronautical literature to collect the published aerodynamic efficiencies of similar-sized, non-copter UAVs. The compiled information allowed a direct comparison of UAVs and gliding birds. Contrary to our expectation, we found that there is no definitive evidence that any gliding bird species is either more or less efficient than a comparable UAV. This non-result highlights a critical need for new technology and analytical advances that can reduce the uncertainty associated with estimating a gliding bird's aerodynamic efficiency. Nevertheless, our survey indicated that species flying within subcritical Reynolds number regimes may inspire UAV designs that can extend their operational range to efficiently operate in subcritical regimes. The survey results provided here point the way forward for research into avian gliding flight and enable informed UAV designs.

1. Introduction

Gliding and soaring are highly efficient modes of transportation for birds, requiring substantially less energy than flapping flight [1–4]. For example, an albatross can soar for thousands of kilometres by exchanging energy from the velocity gradient above the ocean for potential energy, while a hunting kestrel can hang motionless off a cliff on a gusty day [5–7]. This prowess has led many studies to quantify the aerodynamic efficiency of gliding birds, but also to a prevalent belief that gliding birds are more efficient than man-made equivalent gliders. To this end, bird wings are often cited as the inspiration for novel efficient unmanned aerial vehicle (UAV) wing designs [8–10]. Despite the attention within the biological and aeronautical literature, there is no comprehensive survey of gliding bird aerodynamic efficiency nor a direct comparison between birds and modern UAVs. The primary objective of the present work was to review the existing biological and aeronautical literature to compile and compare published estimates of gliding aerodynamic efficiency across all available avian species and modern UAVs. This survey allowed us to contrast the varied methodologies used to estimate avian aerodynamic efficiency and discuss their

differing levels of uncertainty to identify the most reliable estimates of avian aerodynamic efficiency.

In this survey we focussed on aerodynamic efficiency quantified within the context of steady gliding flight rather than soaring flight. The albatross and kestrel both provide examples of soaring flight because they extract energy from the environment, such as the shear layer over the ocean (a form of dynamic soaring) or wind deflected by cliffs (static soaring) [11–13]. Soaring flight is one of the most common forms of non-flapping bird flight where soaring performance is dependent on a flyer's morphology, flight path taken and the velocity gradients in the environment [12, 14]. The latter two parameters are often dictated by an individual's behaviour or local environment. These localized effects make it difficult to identify a standardized performance metric to compare within a species, across multiple species, and to UAVs. In contrast, steady gliding flight is a special case of non-flapping flight where a flyer's performance depends only its morphology. In addition, the aerodynamic efficiency in steady gliding flight is a predictor of soaring flight performance [15]. Thus, we selected to explore avian aerodynamic efficiency through the lens of steady gliding flight to facilitate a comparative approach.

In this work, we first defined an avian gliding flight regime using published flight speed and morphological data (section 2). Next, we defined the equations of motion for steady gliding flight and highlighted the physical underlying assumptions that govern these mathematical equations and their correct implementation (section 3). With the steady gliding flight assumptions in mind, we compared and discussed the existing theoretical (section 4) and experimental (section 5) techniques used to estimate avian aerodynamic efficiency. Due to the wide variety of methodologies implemented over the years, we discussed the uncertainty of each method in detail. Our survey included all available studies on prepared specimens and live gliding birds from wind tunnels or free flight. The data and source for each data point is provided in the supplementary materials (https://stacks.iop.org/BB/16/031001/mmedia). Works that did not indicate the method used to determine the reported aerodynamic efficiencies of birds were not included in this survey [16, 17].

Finally, we performed a survey of all published UAV aerodynamic efficiencies and discussed how these data compare to estimated avian aerodynamic efficiencies (section 6). This comparison was performed using a subset of the published UAV data that operate within the same avian flight regime that was established in section 2. Throughout this work, UAV refers to non-rotary and non-flapping vehicles that fall within class I as defined by the NATO classification (i.e. UAVs with a mass less than 20 kg) [18]. We avoided the term 'fixed-wing' because morphing wing designs, which transition between multiple wing configurations, were included in the literature survey.

2. Avian gliding flight regimes

To enable a comparison between two distinct gliders, it is important to quantify two flow similarity parameters: the Mach number (M) and the Reynolds number (Re). We surveyed the literature to identify studies that reported both non-flapping airspeeds and wing shape parameters to allow a calculation of the range of M and Re used by gliding birds. The ranges were computed from live measurements where birds were observed to hold their wings extended during some portion of the flight and does not include any flapping-only flights. Airspeed measurements from both soaring and gliding flights were included to establish an absolute range of velocities that birds use non-flapping flight. These airspeeds were reported using varied techniques including GPS loggers, rangefinders, radar and wind tunnel studies [1, 6, 7, 19–100, 192].

The first important flow similarity parameter is the Mach number (M), which quantifies the compressibility of the flow. M is the ratio of the freestream velocity to the speed of sound. Defining the M regime is important when travelling close to or above the speed of sound. Gliding birds do not approach this barrier and our review identified the gliding bird M range is between 0.01 to 0.08 (figures 1(a) and (b)). Since gliding bird flight occurs below $M = 0.3$, it can be modelled as incompressible flow [101].

The second important flow similarity parameter is the Reynolds number (Re), which quantifies the ratio of viscous to inertial properties in a flow as defined by:

$$Re = \frac{\rho \bar{c} U}{\mu}, \tag{1}$$

where $\bar{c}$ represents the characteristic length scale, U represents the incoming freestream velocity and, ρ and μ represent the air density and dynamic viscosity, respectively.

Unlike large aircraft or small insects, birds and UAVs operate at an intermediate Re where neither viscous nor inertial effects can be neglected (figures 1(a) and (b)). Specifically, our survey identified that birds glide between a Re of 1.5×10^4 to 5.2×10^5. We chose the mean projected wing chord (projected wing area divided by projected wingspan) as $\bar{c}$ for both birds and UAVs. In the aeronautical literature, $\bar{c}$ is usually chosen as the mean aerodynamic chord (a weighted average of the wing chord along the span). However, most avian studies do not publish the wing chord as a function of span and instead often publish a mean projected chord calculated from a fully extended wing. Because birds have been observed to both increase or decrease their mean projected chord as wind speeds increase, we expect increased uncertainty on the upper Re bound [20, 69].

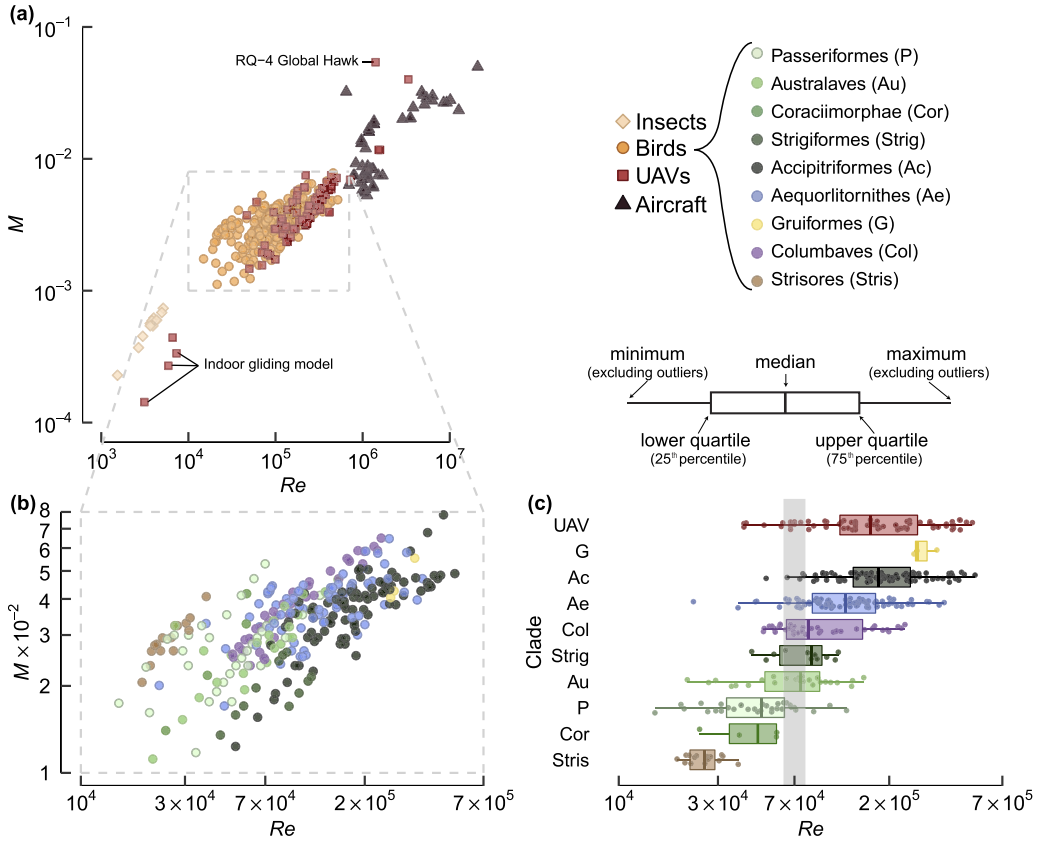

Figure 1. Gliding bird Re and M regimes. (a) Flight regime for gliders. (b) Flight regime for gliding birds coloured by clade. (c) Re regime for each avian clade, the transparent grey line represents the critical Re $\cong 7 \times 10^4$.

Table 1. Phylogenetic grouping of avian species.

Clade	Example species
Galloanserae	*Quail, ducks, geese, chickens*
Strisores	Common nighthawk, swift
Columbaves	Pigeon, wood pigeon
Gruiformes	Common crane
Aequorlitornithes	Gulls, albatrosses, storks, pelicans
Accipitriformes	Hawks, harriers, buzzards, eagles
Strigiformes	Great horned owl, barn owl
Coraciimorphae	Lewis' woodpecker, European bee-eater
Australaves	Falcons, merlins, kestrals
Passeriformes	Starlings, jackdaws, jays, magpies

Next, we separated the collected avian data into clades following the phylogenetic classification established by Prum (figure 1(c)) [102]. Table 1 lists all major clades that are referenced in this work. Clades with large species such as seabirds (Aequorlitornithes) and raptors (Accipitriformes) tend to glide near the upper bound of the Re range whereas small birds such as swifts (Strisores) and passerines (Passeriformes) tend to glide near the lower bound (figure 1(c)). These trends are largely a function of the overall size of the birds within these clades. Figure 2(a) shows Re as a function of the total mass of the bird where the increasing trend is expected because heavier birds tend to have larger mean projected chords ($\bar{c}$) and fly at higher speeds (U) (figure 2(b)) [103].

Our survey does not encompass all avian biodiversity because some birds do not glide and not all birds that do glide have been studied. Of note, the Galloanserae clade is absent since there are relatively few reported gliding speeds (table 1). We identified only one reported gliding measurement from a member of the Galloanserae clade, the barnacle goose (*Branta leucopsis*) gliding at an airspeed of approximately 14.2 m s^{-1} (Re $= 1.5 \times 10^5$ and $M = 0.04$) [104].

Next, we separated the avian Re regime into four sub-regimes that were defined for smooth airfoils by Carmichael (table 2) [105]. Birds glide within subcritical (first two rows) and supercritical sub-regimes (last two rows). In a subcritical regime (Re $\leqslant 7 \times 10^4$), once the laminar boundary layer separates from the surface, the airfoil chord is too short relative to the flow velocity to allow the separated boundary layer to transition to turbulent flow and reattach [105, 106]. This severely degrades performance. Carmichael noted that Re $\leqslant 3 \times 10^4$ the flow is extensively laminar which results in higher aerodynamic efficiency (albeit at lower lift coefficients) than in the higher subcritical sub-regime [105].

The supercritical regimes used by birds are normally characterized by laminar separation bubbles (LSBs). LSBs occur when the laminar boundary layer separates from an airfoil, transitions to turbulent

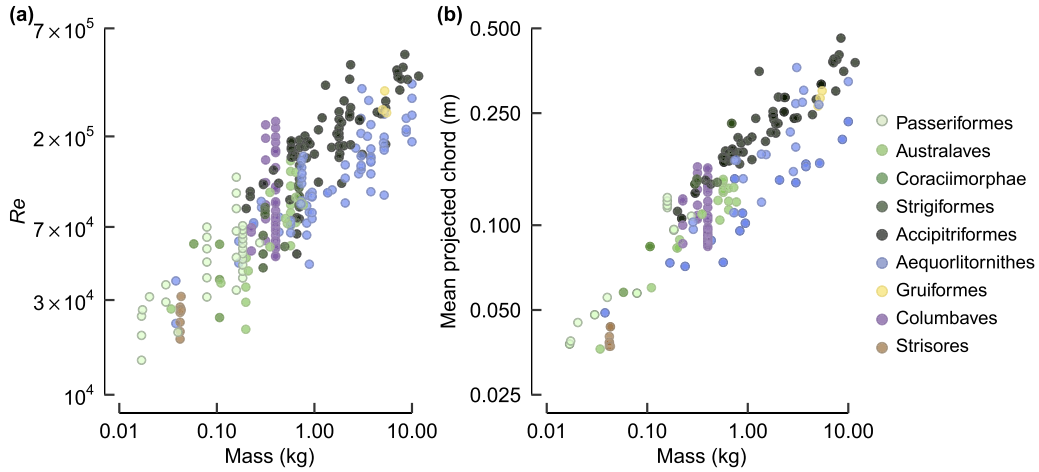

Figure 2. Correlations with body mass. (a) Re and (b) mean projected chord ($\bar{c}$) tend to increase as body mass increases.

Table 2. Re sub-regimes for gliding birds [105, 106, 108]. The dashed line separates subcritical from supercritical regimes.

Re	Clades	Example species
1×10^4 to 3×10^4	Strisores	Swifts (low speed)
	Aequorlitornithes	Small petrel
	Coraciimorphae	Woodpecker
	Australaves	Common kestrel, budgerigar
	Passeriformes	Skylark
3×10^4 to 7×10^4	Strisores	Swifts (high speed)
	Columbaves	Pigeon (low speed)
	Aequorlitornithes	Prion, small petrel
	Accipitriformes	Harris's hawk
	Strigiformes	Barn owl
	Coraciimorphae	European bee-eater
	Australaves	Kestrels, falcons
	Passeriformes	Jackdaw, magpie, woodpecker
7×10^4 to 2×10^5	Columbaves	Pigeon (average speed)
	Aequorlitornithes	Gulls, albatross, large petrels
	Accipitriformes	Hawks, vultures, eagles, osprey
	Strigidae	Barn owl, barred owl
	Australaves	Falcons
	Passeriformes	Jackdaw, magpie
2×10^5 to 7×10^5	Columbaves	Pigeon (high speed)
	Gruiformes	Common crane
	Aequorlitornithes	Storks, pelicans, albatrosses
	Accipitriformes	Large eagles, vultures, condors

flow, and then reattaches to the airfoil as a turbulent boundary layer [106]. The region of separated flow is known as the 'bubble' and degrades wing performance depending on its stability and length [105, 106]. LSBs can be partially or completely eliminated by artificially tripping a laminar boundary layer to transition to turbulent boundary layer. Introducing surface roughness is one way engineers trip a boundary layer and feather roughness has been shown to perform a similar function [9, 107]. For Re $\geqslant 2\times 10^5$, LSBs still exist although the performance markedly improves over the lower regimes [105].

We found that multiple species such as pigeons, falcons and owls bridge the subcritical and supercritical regimes (figure 1(c)). Note that surface roughness may decrease the critical Re and further targeted research is required to determine the mechanisms used by birds that fly in these transitional regimes. Identifying if different tactics are used by the same species at disparate flow conditions may provide a promising avenue of future research for low Re UAVs.

Note that table 2 provides a qualitative description of the flow regimes possibly experienced by gliding birds' airfoils but cannot predict the exact flow characteristics of the wings. Bird wings are three-dimensional, rough, porous, flexible and have a variable chord length. As such, a single bird wing may have airfoils simultaneously operating in multiple Re regimes that do not correspond to the Re regimes experienced by a smooth airfoil. It will be necessary to quantify the true sub-regimes that bird-like airfoils encounter to determine if species are able to transition between sub- and supercritical regimes in flight.

3. Steady glide requirements

It is important to define the assumptions built into a steady gliding framework to support the following discussions on the most reliable method to estimate aerodynamic efficiency. Because gliding is a mode of flight without thrust, we can define the translational equations of motion for the x and z-axes in the inertial reference frame aligned with the body axes of a glider with a body mass (m) as follows (figure 3) [109]:

$$x-\text{axis}: m\dot{U} = -D + mg\sin\theta \tag{2}$$

$$z-\text{axis}: m\frac{U^2}{r_c} = L - mg\cos\theta. \tag{3}$$

Here, U is the airspeed determined by the vector difference between the groundspeed and the local wind vector. The glide angle (θ) is defined between U and the Earth horizon. U_s is the aerodynamic sink speed, which is the difference between the inertial sinking speed and the wind updraft component (for more information refer to Taylor *et al*) [12]. $\dot{U}$ is the acceleration parallel to the flight path and U^2/r_c is the acceleration perpendicular to the flight path given

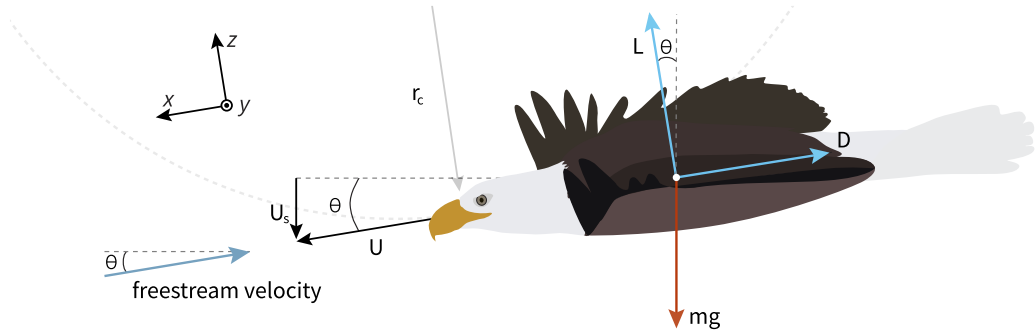

Figure 3. Force balance for steady gliding flight.

by the centripetal force due to path curvature (r_c). These equations of motion assume that the glider will not bank or turn so that all acceleration lies within the x–z plane. If turning or banking were included, there would be an additional equation to account for centripetal acceleration in the y-axis.

Next, for a glide to be considered steady the flight path must be unaccelerated in all axes. This forces the left-hand side of equations (2) and (3) to zero by requiring the airspeed is constant ($\dot{U} = 0$) and the flight path is parallel with the x-axis, ($r_c \to \infty$). Incorporating these two assumptions, we obtain the familiar equation of lift and drag as a function of the glide angle (θ):

$$\left(\frac{1}{(L/D)}\right) = \tan\theta. \tag{4}$$

It can be shown that the maximum range (R) for any given altitude (h) and given wind vector (W) is achieved at the minimum gliding angle ($\theta_{\min}$) and thus $(L/D)_{\max}$ [109]:

$$\left(\frac{R_{\max}}{h_{\text{given}}}\right) = \tan\theta_{\min} = \left(\frac{1}{(L/D)_{\max}}\right) \tag{5}$$

$(L/D)_{\max}$ is a direct measure of the maximum range that a glider can cover for a given height and is the most commonly used metric to quantify a glider's aerodynamic efficiency. Because the velocities are constant, R and h can be replaced in equation (5) by the velocity components in their respective axes to calculate $L/D_{\max}$ as follows:

$$(L/D)_{\max} = \left(\frac{U\cos\theta_{\min}}{U_s}\right)_{\max}. \tag{6}$$

If the glide angle is assumed to be small, this reduces to:

$$(L/D)_{\max} \approx \left(\frac{U}{U_s}\right)_{\max}. \tag{7}$$

To summarize, the critical steady glide assumptions underlying equations (4)–(6) are as follows:

(a) U must be constant ($\dot{U} = 0$),
(b) The flight path must be straight (parallel to the x-axis), and
(c) The measured airspeed must be the true U (i.e. adjusted for all local wind conditions encountered by the bird).

From these equations and assumptions, aerodynamic efficiency can be estimated with one of three distinct methods that we explored in this survey. First, a study could predict $(L/D)_{\max}$ by theoretically estimating the minimum drag for an expected lift condition. Next, a study could experimentally measure U and U_s then use equations (6) or (7) to predict $(L/D)_{\max}$. This requires that the steady glide assumptions are satisfied. Finally, a study could experimentally measure lift and drag forces across a range of flight conditions to directly calculate $(L/D)_{\max}$. These direct force measurements are only dependent on a glider's morphology and the tested Re. To further explore the effectiveness of these varied approaches, we examined the existing theoretical methods (section 4) and experimental methods (section 5).

4. Theoretical determination of avian aerodynamic efficiency

In a steady glide, equation (3) reduces to $L = mg\cos\theta$ and equation (6) can be reformulated to show that:

$$mg/D = \left(U/U_s\right). \tag{8}$$

This simple yet powerful equation is implemented within *Flight*, a popular software developed by Pennycuick that theoretically predicts the aerodynamic efficiency of gliding birds [110]. The advantage of this approach is that it only requires information about a bird's morphology to estimate drag as a function of U. Then, the programme iterates across input U to calculate the associated U_s and then from equation (7) calculates (L/D) at each airspeed. Thus, identifying an estimate for the maximum aerodynamic efficiency and the speed for the maximum efficiency, which is known as the best glide speed.

This methodology is limited by its ability to accurately predict drag. Drag prediction can be simplified if drag is separated into its contributing components. Drag decomposition is non-trivial and

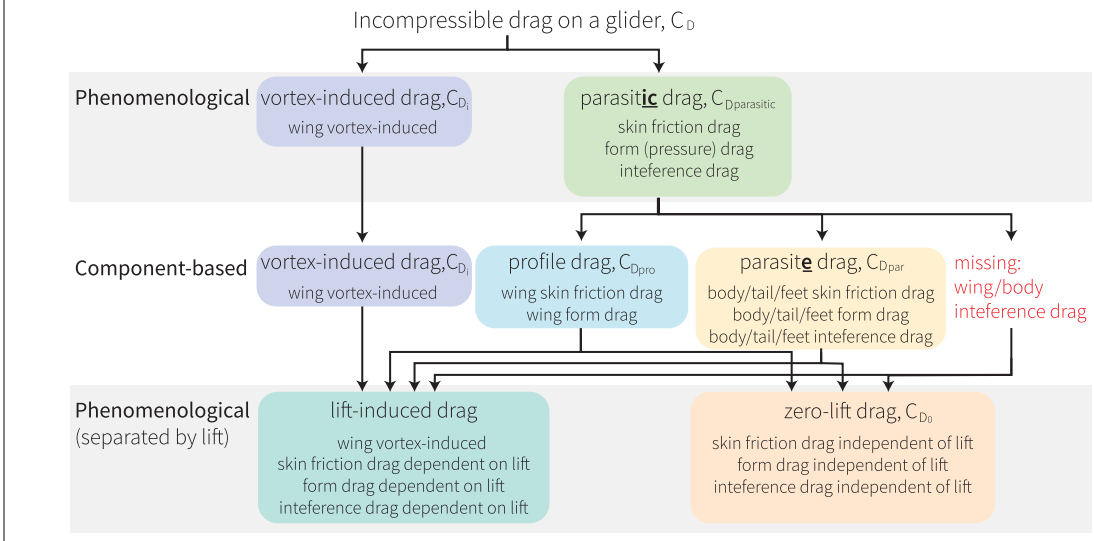

Figure 4. Drag decomposition methods for a glider.

there are many different approaches used by the aeronautical and biological communities. There are three common ways to decompose drag (figure 4). First, drag can be decomposed phenomenologically into vortex-induced drag and parasitic drag [111, 112]. Vortex-induced drag is caused by lift-generated vorticity in the flow and is an inviscid phenomenon [113]. Parasitic drag is due to flow viscosity and includes skin friction drag, form drag and interference drag when gliding in the incompressible M regime [113]. Skin friction drag is a result of the viscous interaction of the flow with the exposed surface of the glider. Form drag, also known as pressure drag, is a result of a pressure distribution caused by the shape of a glider along its length. Finally, interference drag is a result of complex flow interactions between varied components of the glider including the body, wing and tail. Each component of parasitic drag is dependent on lift, thus parasitic drag is not equivalent to zero-lift drag (figure 4) [113].

In contrast, biological literature commonly separates drag into three components based on glider geometry: the vortex-induced drag of the wing, the profile drag composed of the parasitic drag due to the wing and, the parasite drag composed of the parasitic drag due to the rest of the glider (figure 4) [13, 20, 90, 110, 114]. This component-based separation of the drag is particularly useful for flapping flight work. To investigate the assumptions within theoretical estimates of avian efficiency, this paper proceeds using this component-based decomposition of drag, discussing the estimation of vortex-induced drag (section 4.1), profile drag (section 4.2), and parasite drag (section 4.3).

4.1. Vortex-induced drag

Vortex-induced drag is due to the finite nature of wings. At the wing tip, there is no separation between the high-pressure region below the wing and the low-pressure region above. The resulting pressure gradient causes a wing tip vortex that induces a downwards component of velocity (known as downwash) [111]. This additional velocity component sums with the incoming freestream velocity and decreases the effective angle of attack at the location that experiences the downwash. As a result, the lift and drag vectors are rotated such that a component of the lift is oriented towards the trailing edge, parallel to U (figure 3). This component is known as vortex-induced drag, induced drag or vortex drag. Vortex-induced drag is one of the largest contributors to the drag produced by full-scale aircraft and many aeronautical theoretical and experimental studies focus on reducing its effect [112, 115].

One way to minimize vortex-induced drag commonly mentioned within the literature is to increase a glider's aspect ratio (AR), given by:

$$\mathrm{AR} = \frac{b^2}{S}, \tag{9}$$

where b is the wingspan and S is the selected wing reference area. High AR wings are usually associated with lower vortex-induced drag and higher aerodynamic efficiency. This qualitative interpretation requires user caution and an appropriate reference area, which is usually the total wing area for a non-planar wing (refer to appendix A for more details).

The dominant role that AR plays in gliding flight performance analyses is largely due to Prandtl's classical lifting line solution [116, 117]. In 1921, Prandtl published a simple method for predicting the vortex-induced drag of a straight, planar, rigid wing [118]:

$$C_{D_i} = \frac{{C_L}^2}{\pi e_i \mathrm{AR}}. \tag{10}$$

Here, Prandtl derived a span efficiency factor ($e_i \leqslant 1$) that quantifies how closely a planar wing's

lift distribution matches an elliptical lift distribution [119]. An elliptical lift distribution ($e_i = 1$) is the most efficient lift distribution for a planar wing with a fixed span [120, 121]. Note that e_i differs from the Oswald span efficiency factor (e_v) (refer to appendix B for details). As both the Prandtl and Oswald span efficiencies are commonly represented by the same letter (e) we adopted the subscripted nomenclature introduced by Spedding and McArthur for clarity [119]. Commonly, equation (10) is rewritten with an induced drag factor (k_i), where $k_i = 1/e_i$ as:

$$C_{D_i} = \frac{k_i {C_L}^2}{\pi \mathrm{AR}}. \tag{11}$$

Prandtl's equation assumes a rigid, straight, planar wing (i.e. no sweep or dihedral) and is strictly speaking not applicable to bird wings that have spanwise camber, sweep and flexible feathers [111]. Furthermore, some gliding birds have emarginated primary feathers, a splayed thumb feather (alula), or temperature gradients that may induce a spanwise flow [122–128]. It is difficult to include all the complexity of a bird wing into a single model, which challenges the notion that a simple analytical expression for vortex-induced drag is meaningful for bird flight.

In the biological literature, Prandtl's methodology is commonly used with equation (11) and an estimated k_i. However, there are few reliable empirical data to support a prediction of k_i especially for $\mathrm{Re} < 10^5$ [119]. Spedding used lifting-line theory to predict a $k_i = 1.04$ for a gliding kestrel [83]. Commonly in the literature, the magnitude of k_i for bird wings is often estimated to be between 1.1 to 1.2 ($e_i = 0.83$ to 0.91), with the *Flight* software using a default value of $k_i = 1.2$ [20, 76, 90, 92, 110, 129–131]. Recent theoretical work has found that at the best glide speed, the contributions of induced drag will be equal to profile and parasite drag such that k_i could be estimated with accurate predictions of the other two drag components [12]. In all, the implementations of Prandtl's equations have returned useful initial estimates of the vortex-induced drag despite assuming a rigid, straight, planar wing.

In 1962, Cone extended Prandtl's work to predict the minimum induced drag for rigid nonplanar wings with an arbitrary curvature along the span [132, 133]. Using theorems developed by Munk, Cone proposed an equation that is similar in appearance to equation (10) but has a different interpretation of the variables [132]. To avoid confusion with previously established variables, we have adjusted the nomenclature of Cone's original variables as follows [132]:

$$C_{D_{i\,\min}} = \frac{{C_{Lp}}^2}{\pi e_c \mathrm{AR_p}} \tag{12}$$

Equation (12) was developed to compare an optimally loaded nonplanar wing to an optimally loaded equivalent planar wing. The equivalent wing must produce the same amount of lift as the nonplanar wing at the same flight conditions. Furthermore, e_i is replaced with Cone's maximum span efficiency factor (e_c) and, C_{Lp} and $\mathrm{AR_p}$ are from the equivalent planar wing rather than the nonplanar wing. Cone's equation only predicts $C_{D_{i\,\min}}$ for a given wing configuration and cannot be used to predict C_{D_i} for any arbitrary loading condition. This is because e_c is only a constant if the nonplanar wing is optimally loaded such that the lift distribution minimizes the vortex-induced drag for the given geometry [132]. e_c can in interpreted as follows: if $e_c > 1$, an optimally loaded nonplanar wing is more efficient than an equivalent elliptically-loaded planar wing producing equal lift [132]. The reverse is true for $e_c < 1$. Note that e_c does not comment on how similar the optimum lift distribution is to an elliptical lift distribution on the nonplanar wing unlike the e_i interpretation.

Some ambiguity arises when Cone's results are introduced to support the hypothesis that k_i could be less than 1 ($e_i > 1$) for a bird wing [13, 67, 83, 110, 123, 134]. Cone did show that some optimally loaded nonplanar wing configurations could outperform their equivalent planar wing (i.e. $e_c > 1$) but this result does not support the conclusion that $e_i > 1$. This confusion is likely due to overly similar nomenclature between Cone and Prandtl's work. Despite this confusion, recent aeronautical studies have suggested that an effective k_i for nonplanar wings might be less than 1 but, further work is required to reframe Prandtl's analytical equation with respect to a nonplanar wing geometry [10, 135, 136].

Moving forwards, Cone's work should be implemented to predict $C_{D_{i\,\min}}$ and verify the validity of Prandtl's results for nonplanar bird wings. But to correctly predict e_c a bird's optimum lift distribution must be identified. Because birds do not necessarily glide at an optimal loading condition, Cone's equation may be irrelevant for predicting the vortex-induced drag of a live gliding bird [129]. Even for this case, a gliding bird's wing configuration could be analysed with Cone's method to determine its optimum lift distribution and thus its maximum aerodynamic efficiency for the purpose of improving bioinspired design.

Proper identification of any span efficiency factor requires knowledge of the lift distribution used in gliding bird flight. Promising advances in flow characterization and sensing technology have provided measures of force distributions in flight. One study placed pressure sensors along the wing of a Canada goose during take-off to directly measure the pressure distribution on the wing [137]. This technique has not yet been implemented in gliding flight. Particle imaging velocimetry (PIV) has provided some of the first experimental quantification of a live bird's lift distribution by measuring the downwash produced by gliding raptors [138]. Interestingly, the downwash

distribution did not support an elliptical lift distribution and the authors suggested the gliding raptors used lift distributions with a constant sectional coefficient of lift or possibly a bell-shaped lift distribution.

Previous work has implicated the bell-shaped lift distribution as the lift distribution used by gliding birds [139]. Prandtl showed that vortex-induced drag is minimized with a bell-shaped lift distribution when the weight (implemented as total produced lift) and the lift moment of inertia is held constant during optimization rather than the wingspan [120, 121]. Note that the optimal wing with a bell-shaped lift distribution would have a span that is 22% longer than the elliptical wing. Other optimal lift distributions have been identified by holding different wing properties constant throughout optimization [140]. This suggests that if it is possible to identify the physical attributes (weight, maximum stress, wing loading, etc) that have been constrained throughout the evolution of bird wings, it may be possible to estimate which lift distribution would be optimal for the wing shapes of modern birds. Such an estimate may provide a useful starting point but would not be expected to be the true lift distribution used by gliding birds because evolution does not specifically optimize for minimum vortex-induced drag, efficient gliding flight or even flight at all [141].

The analytical methods discussed herein improve our ability to estimate a bird's vortex-induced drag, but it is important to keep in mind that these analytical methods can be enhanced with numerical techniques. Higher fidelity numerical methods have improved accuracy over classic analytical equations for rigid nonplanar wings and should inform future analyses [135, 136, 142]. Currently, there are relatively few studies that leverage computational fluid dynamics (CFD) methods while analysing a bird wing. This is likely due to the computational cost of modelling a complex bird wing or the many wing configurations that a single bird can assume while gliding. Thus, analytical equations remain especially important to make meaningful inferences about the vortex-induced drag in gliding bird flight.

4.2. Profile drag

Profile drag includes parasitic drag on a wing independent of the vortex-induced drag (figure 4) [143]. Profile drag as defined here is dependent on lift because lift increases the skin friction and form drag on an airfoil's upper surface [113, 115]. Profile drag is quantified with the profile drag coefficient:

$$C_{D_{\text{pro}}} = \frac{D_{\text{pro}}}{1/2\rho U^2 S}. \tag{13}$$

A bird's profile drag is usually determined with wake measurements or as the difference between an experimentally measured drag and the estimated vortex-induced drag and parasite drag contributions. Wake measurements on flying animals are sensitive to the method that they are acquired, which is discussed in more detail by Dabiri [144]. It is challenging to experimentally eliminate the contributions of vortex-induced drag or wing–body interference drag from a wake-based analysis. Whereas the subtraction-based method relies on an accurate prediction of vortex-induced drag and parasite drag, both of which require many assumptions (sections 4.1 and 4.3) [143].

PIV measurements on prepared osprey (*Pandion haliaetus*) wings predicted that the profile drag was responsible for 15%–30% of the total body drag and that the contribution of form drag was two to six times larger than the skin friction contribution [145]. The sectional $C_{D_{\text{pro}}}$ measured at cross-sections along the wing was 0.03 to 0.06 for the osprey specimen and 0.02 to 0.03 for a live Harris' hawk (*Parabuteo unicinctus*) [143, 145]. The hawk measurement was within a similar range that was obtained using the subtractive method albeit with very high data scatter [143]. The entire wing $C_{D_{\text{pro}}}$ was found to vary between 0.01 to 0.03 for a live gliding western jackdaw (*Corvus monedula*) and 0.01 to 0.05 for a live gliding common swift (*Apus apus*) [20, 129, 146]. Numerical methods should be used to further validate these experimental results. For simplicity in theoretical calculations, the profile drag coefficient is often assumed to be a constant value around 0.02 (*Flight* software defaults to $C_{D_{\text{pro}}} = 0.014$), or a function of Re based on the skin friction drag on a flat plate [12, 110].

4.3. Parasite drag

Parasite drag includes parasitic drag on the rest of the glider (figure 4). It is nondimensionalized by a bird's body frontal area (S_{b}) rather than the wing reference area [114]:

$$C_{D_{\text{par}}} = \frac{D_{\text{par}}}{1/2\rho U^2 S_{\text{b}}}. \tag{14}$$

Quantifying avian parasite drag has been of great interest and controversy over the years [12, 114]. Early studies on prepared bird body specimens found relatively high body drag coefficients from 0.2 to 0.4 [69, 90, 114, 147]. However, a wind tunnel analysis of flapping birds estimated that the body drag coefficient must be significantly lower ($C_{D_{\text{par}}} = 0.08$) for the cruise speed to match the estimated minimum power velocity [148]. Note that this estimation was done during flapping flight and extended to apply to gliding flight because the estimated minimum power velocity is rooted in helicopter theory [149]. Later an experiment on diving passerine birds estimated a range of $C_{D_{\text{par}}}$ from 0.08 to 0.4 while a wind tunnel experiment on common swifts estimated a range from 0.2 to 0.3 [20, 146, 150, 151]. Finally, two separate experiments on starling bodies found that the parasite drag was responsible for 4%–14% ($C_{D_{\text{par}}} = 0.2$ to 0.4) of the total drag on a prepared European starling (*Sturnus vulgaris*) specimen [114, 151, 152].

$C_{D_{\text{par}}}$ is usually estimated as a constant around 0.1, which now the default for the *Flight* software [110].

Although parasite drag is dependent on lift, a constant $C_{D_{par}}$ is likely a fair approximation because it is widely agreed that the magnitude decreases only slightly for large increases in Re [114, 129, 131, 153–155]. But the use of a constant $C_{D_{par}}$ across different bird species is debatable [110]. Heavier birds have proportionally wider and flatter bodies [156]. Increased elliptical shape provides a streamlining effect that likely reduces form drag for supercritical regimes [157, 158]. These trends suggest that form drag could be more important for heavier birds that fly in a supercritical regime.

4.3.1. Interference drag

Another factor that contributes to the variable range of $C_{D_{par}}$ is the interference drag of the body and other components of a bird. The body/tail/feet interference drag is included within the traditional prepared specimen measures of parasite drag. The effect of the feet is to act as an airbrake significantly increasing the overall drag [69]. To estimate the maximum aerodynamic efficiency, the feet are assumed to be 'tucked-in' and covered by covert feathers [110].

The literature shows conflicting effects of body–tail interactions. One study on a starling body found that the presence of a furled tail decreased $C_{D_{par}}$ by 25-55% and a separate study on starling bodies showed that the presence of a spread tail increased $C_{D_{par}}$ for the same angle of attack [152, 159]. In flapping flight, the presence of a tail on a flapping black cap (*Sylvia atricapilla*) increased total drag, but had no effect for a thrush nightingale (*Luscinia luscinia*) [160]. Because some of the initial estimates used to refine calculations of parasite drag also came from a flapping flight analysis, it would be informative for future parasite drag studies to contrast gliding and flapping flight body postures within the same species.

The commonly implemented component-based drag decomposition overlooks interference drag between the wing, body and tail. Wing–body interference drag has been implicated as major component of a bird's overall drag [114, 152, 159]. This is in part due to the ability for a bird's body to produce lift, albeit much less than the wing. Body-only models and body–tail models of a starling produced approximately 5.5% and 25.8% respectively of the total lift produced by a full model [114, 138, 152]. As a result, there is a pressure difference between the top and bottom producing vortex-induced drag on the body [114, 138]. In fact, flow visualizations of body–tail models have demonstrated a 'scarf' vortex on the body that separates at the neck and has trailing vortices running along either side of the body [114]. These vortices would likely be interrupted by the presence of wings on the body–tail model [110, 152]. Measurements on starlings have shown that at low body angles of attack, the addition of wings at low incidence angles tend to reduce the body drag coefficient compared to a body-only model [151]. This suggests that measuring parasite drag on an isolated bird body does not accurately capture the drag characteristics in live gliding flight. Regardless, predicting the wing–body interference effects is notoriously difficult even for a conventional aircraft [109]. PIV measurements or high-fidelity numerical models will be highly valuable to further quantify the implications of interference drag for gliding birds.

4.4. Theoretical prediction of aerodynamic efficiency

The *Flight* software estimates drag as a summation of vortex-induced, profile and parasite drag computed using the assumptions discussed above [110]. To summarize, vortex-induced drag is estimated using Prandtl's equation with a constant k_i across species. Profile drag and parasite drag are estimated as a constant across species and Re. Pennycuick improved these estimations by incorporating a parameter that accounts for a bird's variable wingspan [110]. This programme is commonly used to estimate a bird's best glide speed and then compare to the true measured gliding airspeeds, which has had varied success across different species and studies [12, 14, 103, 161].

Flight is not the only theoretical method that estimates the drag on avian wings to predict the aerodynamic efficiency. Differing equations have been developed by Pennycuick in earlier work, Tucker, Eder and others following similar approaches [35, 68, 90]. It is also common to use an energy conservation formulation of gliding flight that balances potential energy with the energy lost due to drag [12, 90, 110, 162, 163].

For the same bird, different analytical equations have yielded significantly different estimates of aerodynamic efficiencies [131]. For example, the $(L/D)_{max}$ of a wandering albatross (*Diomedea exulans*) has been predicted to be 14, 21 and 23 by three different calculations [6, 68, 90]. The model developed by Tucker (albatross $(L/D)_{max} = 14$) provided a prediction that matched a wind tunnel measurement for a black vulture, but overpredicted the efficiency for a laggar falcon (*Falco jugger*) by 19% [66, 90, 92]. In both cases, Tucker's model underpredicted the best glide speed by 2 m s^{-1}. In addition, theoretical methods have returned some of the highest estimated avian aerodynamic efficiencies (figure 5(a)). Combined with the significant discrepancies between models, our survey results suggest that theoretical estimations are useful to produce an initial efficiency estimate. However due to the critical underlying assumptions in the drag prediction methods, these models should not be considered final without experimental or numerical validation.

5. Experimental determination of avian aerodynamic efficiency

Due to the assumptions within and discrepancies between theoretical models, it becomes important

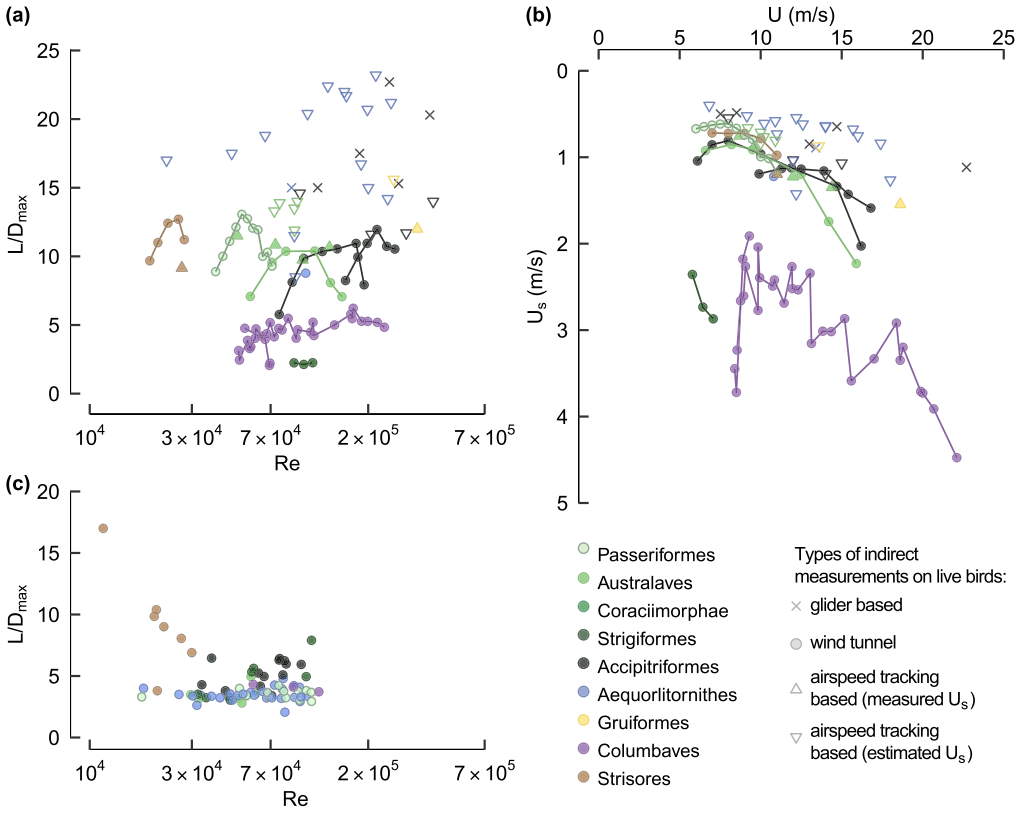

Figure 5. Aerodynamic efficiency of gliding birds. (a) Aerodynamic efficiency of gliding birds from velocity measurements, the solid lines connect measurements on the same individual (b) estimated glide polar (c) aerodynamic efficiency of prepared wings from wind tunnel force measurements.

to leverage experimental results to advance our understanding of avian gliding efficiency. Multiple studies have quantified the aerodynamic efficiency of live gliding birds, prepared specimens or manufactured bird replicas. Here, we reviewed estimates from three types of methodologies. First, in section 5.1 we discuss velocity measurements on freely gliding birds, where U and U_s is measured. Next, in section 5.2 we discuss velocity measurements on birds flying in a wind tunnel. In section 5.3 we briefly reviewed the progress made to gain direct force measurements from a live bird, but there are currently no published results. Finally, in section 5.4 we discuss direct force measurements of prepared or manufactured bird specimens. Figures 5(a) and (b) contain all of the data collected during our survey of a full bird's aerodynamic efficiency [1, 6, 7, 19, 20, 23, 34, 35, 47, 50, 51, 57, 60, 66–71, 76, 90–92, 164] and figure 5(c) contains all data on wing-only aerodynamic efficiency [130, 165–169].

5.1. Velocity measurements on freely gliding birds

While both velocity and force measurements can be used to predict L/D_{max} of a freely gliding bird, it is most pragmatic to measure the velocity of a live bird rather than the produced aerodynamic forces. Yet, this presents its own set of challenges because the steady glide assumptions must be satisfied throughout the measurements. The two common methods used to measure a bird's airspeed include glider-based measurements and rangefinder or radar tracking measurements.

From the 1920s to the 1970s, sailplanes flew behind freely gliding birds and estimated the birds' airspeed and sink speed based on those of the sailplane [50, 67, 71]. Using equation (7) and thus a small glide angle assumption, the pilots could estimate the birds' $(U/U_s)_{max}$ and $(L/D)_{max}$ [67]. These measurements returned the highest experimentally measured avian lift-to-drag ratios (figure 5(a)). Unfortunately, this technique is prone to errors based on differences in U and the flight path between the bird and the glider, which makes it difficult to ensure that the three steady glide assumptions are satisfied. Additionally, instrumental and analysis uncertainties alone yields an estimated U error of $\pm 10\%$ [67, 92]. A possible magnitude for overprediction of this method is demonstrated by two independent studies on gliding black vultures (*Coragyps atratus*). At Re $\cong 2 \times 10^5$: a glider-based study reported $(L/D)_{max} \cong 23$ while a wind tunnel study on a live bird reported $(L/D)_{max} \cong 12$ [66, 71]. As such, glider-based measurements are expected to overpredict a bird's aerodynamic efficiency in an unreliable fashion.

Tracking technologies such as radar and rangefinders have enabled sophisticated U and U_s measurements of freely gliding birds [35, 70, 162, 170]. These tools, combined with anemometers

and weather balloons, have provided increasingly accurate estimations of a gliding bird's velocity [82, 155]. Like glider-based studies these measurements must satisfy the steady glide assumptions, and it is difficult to identify the local velocities encountered by a gliding bird. Most studies are performed on calm days to minimize these errors. The rangefinders commonly used in modern studies have a distance accuracy of ± 2 m to ± 5 m [155, 171]. This gives a relatively high instrumental uncertainty range which compromises the ability to ensure that the second steady glide assumption is satisfied. More recent technological advances have further reduced measurement error by minimizing the equipment error [47]. A study on gliding common swifts using rotational stereo videography observed that the swifts in a straight, unaccelerated glide, had a $(L/D)_{max}$ of approximately 9.2. This value is only slightly lower than wind tunnel estimates on live swifts ($(L/D)_{max} = 12.7$) and wind tunnel estimates on prepared wings ($(L/D)_{max} = 10.4$) (figure 5(a)) [47, 167, 172]. However, the study noted that the birds appeared to use environmental energy during measurements. This makes it difficult to satisfy the third steady glide assumption. Thus, it remains a substantial challenge to ensure that efficiency estimates based on a tracked bird velocity satisfies the steady glide assumptions.

Recent studies have mounted inertial systems onto freely flying birds using a pitot tube to directly measure the true airspeed of the bird [12, 73, 173, 174]. This methodology allows researchers to ensure that all three steady glide assumptions are satisfied throughout a measurement. One study implemented onboard devices on a steppe eagle (*Aquila nipalensis*) including a pitot tube, barometer and GPS logger [12]. With this data they were able to reliably determine the airspeed of the birds in steady gliding flight. Interestingly, their results showed very good agreement with a previous radar tracking study lending credence to this simpler technique [12]. This method has not yet been used to estimate a bird's $(L/D)_{max}$ but provides a promising avenue for future work.

5.2. Velocity measurements on birds gliding in a controlled environment

The uncertainty associated with velocity measurements can be reduced by relocating a bird from the complex natural environment to a controlled environment such as a wind tunnel or an indoor flight corridor. In these studies, it is possible to ensure that a bird performs a steady glide. For these experiments, it is common to use a tilting wind tunnel with an open test section to determine the minimum glide angle of a bird [20, 66, 69, 76, 85, 91, 92]. This is usually done by manipulating the angle of the tunnel until a minimum angle is found where the bird will perform an equilibrium glide for a given airspeed. This angle is reported as the minimum glide angle (θ_{min})

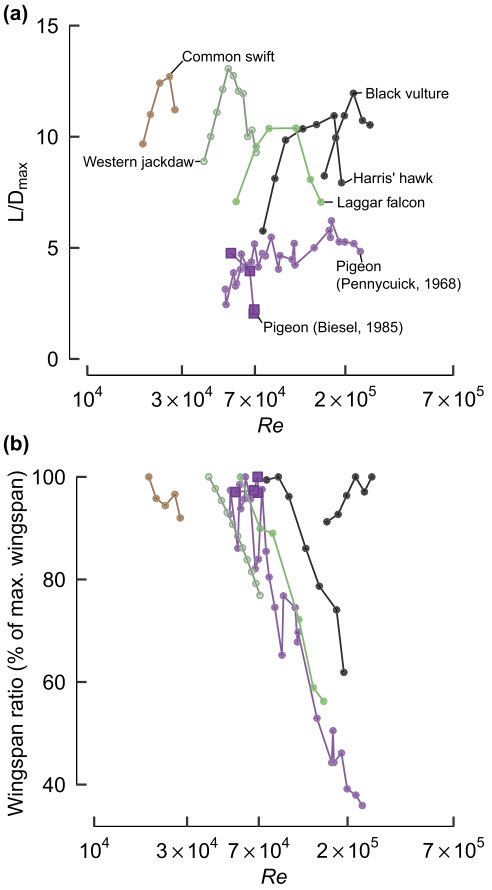

Figure 6. Implications of avian wing morphing. (a) L/D_{max} for each tested Re. (b) Ratio of the wingspan used at L/D_{max} to the maximum wingspan.

of the bird so that equation (5) returns L/D_{max}. The measurement error on $(L/D)_{max}$ is estimated to be relatively small at approximately ± 0.03 or 0.2% in one study although the uncertainty introduced by low Re effects are difficult to quantify [20]. Because all steady glide assumptions are satisfied and the instrumental error is low, wind tunnel measurements represent reliable estimates of avian aerodynamic efficiency [20]. Further support is provided by two separate experiments on pigeons that found good agreement between $(L/D)_{max}$ for a specific U [69, 100].

Contrasting these two pigeon studies highlights a major challenge in performing live bird wind tunnel studies. In one study, the pigeon increased its mean chord with velocity where the other individual reduced its mean chord [69, 100]. This results in an opposite relationship of $(L/D)_{max}$ with Re for these two individuals even though the responses to U are indistinguishable (figures 5(b) and 6(a)). Because practical and ethical considerations limit wind tunnel investigations to a small sample size, the results will be dependent on that individual birds' reaction which may or may not be representative of the entire species.

Furthermore, it is difficult to decouple behaviour from maximal capability when working with live animals. For example, after a certain minimum angle the birds would not glide and returned to flapping

[66, 69, 85, 91, 92]. While this provides a measure of the lowest angle that the individual bird will perform a glide, it is not possible to determine if this is due to the species' physical inability to perform a steady glide at a lower glide angle or a behavioural choice to return to flapping flight [100]. Given this behavioural constraint, wind tunnel studies return an estimate of a bird's highest minimum glide angle. This result in turn dictates a lower bound on a species' aerodynamic efficiency.

Freestream turbulence is another important contributing factor in any wind tunnel measurement of aerodynamic efficiency. Increased turbulence intensity in a bird's Re range induces flow to transition from laminar to turbulent [175, 176]. This transition results in a shorter and thinner LSB, leading to improved aerodynamic performance on smooth airfoils. Wind tunnel tests on prepared gull wings also found aerodynamic efficiency increased as the turbulence intensity increased [165]. Most modern avian studies use low turbulence wind tunnels, but wind tunnel studies on live birds require a net to avoid the bird flying into the contraction chamber. The net can increase the turbulence intensity to around 1% of the mean flow velocity [76]. This increase in turbulence intensity will increase the measured aerodynamic efficiency on live birds over theoretical predictions. Therefore, it is important to compare flight performance characteristics across a consistent level of turbulence intensity [20, 167].

5.2.1. Effect of wing morphing

Wind tunnel measurements on live gliding birds provide a secondary benefit because they allow us to investigate how wing morphing affects avian aerodynamic efficiency. It is well documented that many gliding birds, including gulls, pigeons, swifts, storks, hawks, and falcons will flex their wing joints to reduce their wing span as wind speeds increase [20, 35, 66, 69, 85, 91, 165]. It has been hypothesized that this allows speed control by reducing lift production and geometric twist to avoid high aerodynamic loads on the wing [12, 110]. Joint flexure reduces the projected wing area, which is linearly related to the wingspan for all tested birds [66, 69]. Wrist and elbow flexion are largely responsible for the majority of the observed shape change [85, 165]. For swifts, wrist flexion shifts $(L/D)_{max}$ towards a higher airspeed while decreasing the magnitude [167]. Note that some species such as black-billed magpies (*Pica hudsonia*) do not morph their wings as wind speeds increase, instead increasing the frequency of bounding flight (where the wings are held close to the body between flapping bouts) [85].

To investigate the implication of wing morphology and flight conditions on aerodynamic efficiency, we compiled data from seven studies that have quantified the aerodynamic efficiency of a live bird in a wind tunnel while noting the wingspan, projected wing area, and airspeed (figure 6) [20, 66, 69, 76, 91, 92, 100]. These studies include wind tunnel velocity measurements from a live common swift, western jackdaw, black vulture, Harris' hawk, laggar falcon and pigeons. When gliding at their minimum glide angle for each velocity, most individuals reduced their wingspan as Re increased (figure 6(b)). The falcon, jackdaw and swift also folded their tail as Re increased, further reducing the wetted surface area of the bird. Pennycuick's pigeon had a nearly constant tail area, suggesting the pigeon maintained a folded tail throughout the entire tested range [69]. Unlike all other measured species, as Re increased the black vulture increased its wingspan and wing area when gliding steadily at the minimum glide angle [66]. Since vultures fly near the upper Re range of the investigated birds (figure 1(c)), it is possible that this behaviour is due to a growing role of vortex-induced drag at higher values of Re. This hypothesis requires further investigation but suggests that future morphing wing UAVs would benefit from analysing the differences between morphing behaviours of small and large bird species.

5.3. Force measurements on freely gliding birds and gliding birds in a controlled environment

Technology is trending towards the ability to directly measure the aerodynamic forces acting on a gliding bird in a controlled environment (be it a wind tunnel or flight arena) but, this is by no means a simple endeavour [20, 138, 146, 177]. Future studies will make use of PIV measurements, aerodynamic force platforms and/or direct pressure sensors installed on birds' wings [137, 138, 178]. As it stands, there are no published direct force measurements of L/D_{max} on a gliding bird, although PIV has been used to estimate the induced drag, profile drag and parasite drag from the wake [129, 146, 172, 179]. As the use of these advanced technologies becomes more widespread, direct measurements of the aerodynamic efficiency of a live gliding bird will become more prevalent and allow validation of other techniques.

5.4. Force measurements on prepared bird specimens

Wind tunnels can also be used to directly measure the aerodynamic forces on bird specimens (prepared using taxidermy techniques) or replicas [180–182]. The advantage to this method is that it allows a direct measurement of L/D_{max} and removes behavioural considerations. However, when preparing specimens, it is not possible to guarantee that a bird's true gliding posture has been replicated.

Full bird specimens have only been investigated a few times in a wind tunnel. These studies reported a low L/D_{max} around 4 for both an Alsatian swift and black kite (*Milvus migrans*) and 5.6 for a starling [152, 180, 182]. One author reasoned that these low results could be caused by active control of feather flexion in flight [180]. Indeed, a wooden model of a gull in a gliding flight configuration estimated a highly

efficient flight with an L/D_{max} of 14.3 [181]. The model did not include feathers thus allowing an experimental investigation of the true gull shape without the confounding factors introduced by feathers. Future studies that contrast results between prepared specimens, model birds and freely gliding bird studies will be necessary. Identifying the discrepancies between models and live birds may enhance our understanding of the active controls used by gliding birds.

Multiple wind tunnel studies on prepared wings have been performed over the years. Studies on half-span bird wings have measured significantly lower $(L/D)_{max}$ than expected from wind tunnel measurements on live birds (figure 5(c)) [130, 165, 166, 168, 169]. For example, a western jackdaw wing measured a $(L/D)_{max}$ that was 68% lower than the live wind tunnel measurement [76, 169]. To date, only one isolated wing measurement reported a higher aerodynamic efficiency than the full bird; Withers found that a half-span common swift wing had an $(L/D)_{max}$ of 17, which is 34% higher than the live wind tunnel measurement [20, 130]. However, a separate study on full-span common swift wings estimated an $(L/D)_{max}$ of 10.4, 18% lower than the live wind tunnel measurement [20, 167]. The discrepancies may be the result of wing preparation or experimental methodology. In all, the wing-only measurements indicate that the full bird aerodynamic efficiency is likely higher than the wing-only efficiency.

This conclusion differs from conventional aircraft, where the addition of an aircraft body tends to increase total drag and only slightly increase lift, while the addition of a conventional tail increases drag and decreases lift. Thus, the addition of a conventional tail and fuselage serves to reduce the overall aerodynamic efficiency. A conventional tail's negative lift production is necessary for pitch stability when the centre of gravity is aft of the aerodynamic centre [109]. It follows that if a bird's aerodynamic efficiency increases, rather than decreases, with the addition of a body and tail, then the avian body and tail do not have the same aerodynamic force production as conventional aircraft. Recent PIV measurements agree with this hypothesis as they confirmed that the tails of two owl species and a goshawk (*Accipiter gentilis*) do not act as conventional aircraft tails, because they produced significant positive lift while gliding [138]. By extending this analysis to more species across varied flight conditions, we can further investigate the role of the tail in gliding flight.

5.5. Summary of the estimated avian aerodynamic efficiency

Finally, we can compare all published avian aerodynamic efficiencies estimated with both theoretical and experimental techniques (figure 5(a)). We found that the highest predicted avian efficiencies belong to Pennycuick's theoretical predictions of seabird efficiencies including albatrosses and petrels [36, 68]. Their high efficiency continues well into the subcritical range where the Wilson's storm petrel (*Oceanites oceanicus*) is predicted to be more efficient than a common swift. Although it is likely that seabirds such as albatrosses are highly efficient, recall that Tucker's analytical model yielded an efficiency for an albatross that was 40% lower than Pennycuick's estimate bringing the accuracy of these very high efficiencies into question [68, 90].

Only glider-based studies and theoretical results have predicted avian efficiencies above $(L/D)_{max} = 14.3$ [6, 15, 19, 35, 50, 67, 68, 70, 71]. After these measurements, the highest aerodynamic efficiency is from the wind tunnel measurements on a carved wooden gull that returned an $(L/D)_{max}$ of 14.3 [181]. For the advanced tracking techniques discussed in section 5.1.2 the highest measured $(L/D)_{max}$ was 12 from a common crane [70].

Examining all reported avian efficiencies highlights the need for estimates of U_s to be highly sensitive. Using all reported efficiency estimates, we determined that the minimum U_s for a steady gliding birds falls between 0.4 m s^{-1} to 3 m s^{-1}, with the majority of species falling at or below 1 m s^{-1} (figure 5(b)) [57, 68]. This small range suggests that theoretical methods reliant on U_s predictions (such as *Flight*) and experimental direct measurements of U_s must provide accurate estimations on the order of 0.01 m s^{-1} to differentiate between species. As the expected efficiency increases, U_s measurement accuracy must increase accordingly.

Our survey identified that measurements on live birds in a controlled environment provide the most reliable measure of aerodynamic efficiency. The highest aerodynamic efficiency from a wind tunnel study is from the swift and western jackdaw both with an $(L/D)_{max}$ of approximately 13 [76, 172].

6. Comparison to UAV efficiency

The consolidated results on avian gliding aerodynamic efficiency can now be compared to non-copter UAVs that fly in a comparable Re and M number regime. We further limited the identified UAVs to those that had control surfaces. Unlike birds, who can switch between powered (flapping) and gliding flight, most of the UAVs in our survey are continuously powered by a propeller. In this case, quantifying aerodynamic efficiency takes on a secondary use because the maximum range of a propeller-driven aircraft is also directly proportional to $(L/D)_{max}$ [109].

The identified UAVs in our study had wing loadings and a total mass on the same scale as birds (figures 7(a) and (b)) [21, 26–28, 30, 33, 36–38, 40, 48, 54, 80, 81, 89, 96]. However, multiple UAVs were lighter than birds that flew at similar Re, including Aerovironment's Black Widow and the Colorado MAV [38, 40]. One heavier exception was

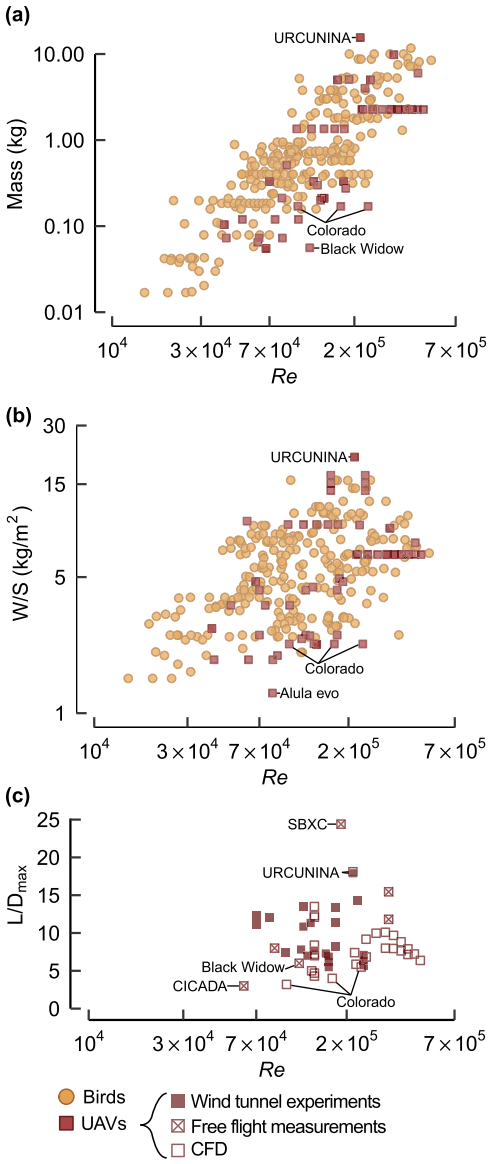

Figure 7. Selected UAVs for comparison to birds. (a) UAV and bird masses (b) UAV and bird wing loading (c) UAV aerodynamic efficiency by measurement type.

the URCUNINA-UAV, which weighs 16 kg and has a wing loading of 21 kg m^{-2} [27].

As with gliding birds, there are many different methods to predict UAV aerodynamic efficiency. Our literature survey included force measurements from wind tunnel experiments, velocity measurements from onboard equipment in free flight, and numerical predictions from CFD methods. The uncertainty of each method can be highly variable, and we will briefly mention some key contributors for each method. Beginning with wind tunnel data, experiments at low Re have an estimated $(L/D)_{max}$ uncertainty of $\pm$8.5%, although the uncertainty will depend on the experimental setup [183]. Estimates from free flights are subject to higher uncertainty than wind tunnel or numerical results, where even UAVs specifically designed for meteorological applications have a reported velocity measurement error of 0.02 m s^{-1} to 0.5 m s^{-1} [184]. Although these errors are higher than the 0.01 m s^{-1} accuracy required to differentiate between species, these errors are expected to be lower than the tracking-based measurements on free flying birds due to the ability to ensure the steady glide assumptions are satisfied with onboard velocity measurements. Numerical predictions using vortex lattice methods (VLM) are often calculated using XFLR5. This method is successful for initial design purposes but it underpredicts the total drag and overpredicts the aerodynamic efficiency [185]. VLM solutions have been removed from the analysis because of the high associated uncertainty. CFD is a more reliable, though more computationally expensive solution. Errors in CFD analyses can arise due to numerical discretization and uncertainty within the model itself. For further details, refer to reviews by Najm and, Oberkampft and Blottner [186, 187]. In all, we expect that data from free flights, CFD, or wind tunnel measurements provide a reliable estimation of a UAV's aerodynamic efficiency (figure 7(c)).

Our survey found that the aerodynamic efficiency of UAVs that fly in the same regime as birds, ranges from an L/D_{max} of 3–14 with a few exceptions (figure 7(c)). The URCUNINA-UAV and an SBXC glider have high reported efficiencies with L/D_{max} of 18 and 24, respectively [27, 36]. This is not a surprise as URCUNINA-UAV was designed for volcano monitoring and utilizes a pusher propeller configuration while the SBXC is a hand-launched unpowered glider. Keep in mind that the URCUNINA-UAV has a higher wing loading than an equivalent bird, which indicates a lower stall speed. Stall speed refers to the minimum velocity that a flyer can operate in steady, level powered flight and does not relate to a gliding flight condition.

The aerodynamic efficiency of a bird can now be directly contrasted against the efficiency of comparable UAVs (figure 8). For completeness, figure 8(a) includes all published estimates of avian and UAV aerodynamic efficiency. However, given the associated uncertainty that we identified with theoretical predictions and glider-based studies, we limited our avian data points to only wind tunnel measurements (figure 8(b)). With this reduced data set, we found that there was at least one UAV design that had a higher aerodynamic efficiency than any measured bird operating within the same supercritical Re sub-regime. This observation is based on the airfoil sub-regimes defined by table 2 with divisions demarcated by the x-axis ticks in figure 8(b). As discussed in section 5.2, these avian data points represent a minimum bound on aerodynamic efficiency and it is possible that these birds are physically capable of more efficient glides.

If we reconsider the full dataset in figure 8(a), it remains possible that birds can outperform UAVs operating within supercritical regimes. Note that even with the full dataset, a UAV (the SBXC) is still the most

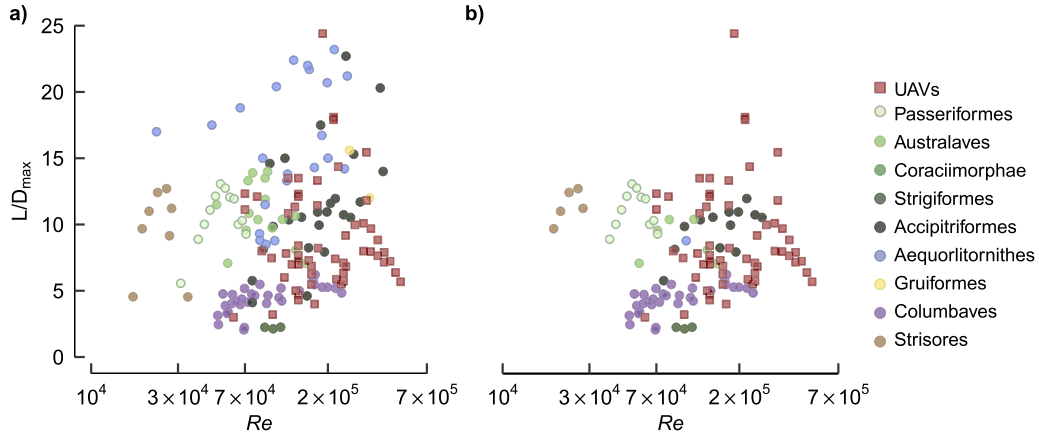

Figure 8. Aerodynamic efficiency of birds compared to UAVs. (a) All published avian efficiency metrics (b) avian efficiency measurements from wind tunnel only.

efficient glider in our study [36]. Unfortunately, we found high uncertainty in the published avian theoretical estimates and that wind tunnel results have not been able to measure birds that are expected to be highly efficient (such as an albatross). Therefore, we cannot state with absolute certainty that birds are more or less efficient than UAVs in the supercritical Re regimes. At best it can be noted that the efficiency of birds and comparable UAVs in supercritical Re regimes appear to be within a similar range.

We only were able to identify one comparable UAV with a published aerodynamic efficiency metric operating in the subcritical Re regimes. This is possibly because the subcritical regimes are dominated by rotary or flapping wing designs. The CICADA UAV (a low-cost, disposable glider) with an $L/D_{\max} = 3$ substantially underperformed the western jackdaw, laggar falcon and swift that fly within this same regime (figure 8(b)) [20, 37, 76, 92]. Subcritical UAVs are often designed to maximize their wing area (thus maximizing the wing chord for a fixed wingspan) to provide controllability and stability at the expense aerodynamic efficiency [64]. In addition to stability requirements, the CICADA and other fixed-wing UAV designs must satisfy constraints on their geometry such as the need to stack easily within a specified enclosure [37]. Unlike the CICADA, the jackdaw and falcon can morph their wings to both adjust their stability characteristics and fold their wings flat to their body when needed [165, 188]. It is likely that birds' adaptable wing geometry allows geometric and stability constraints to be satisfied without needing to sacrifice performance when flying in these subcritical regimes.

6.1. Differences in aspect ratio used by UAVs and birds

To further explore possible differences in wing geometry, we compiled the aspect ratio of each bird and comparable UAV. Our survey revealed that the projected AR of birds tends to be higher than the projected AR of most comparable UAVs (figure 9(a)) [1, 6, 7, 19, 22, 29, 34, 35, 39, 45, 47, 49–51, 57, 59, 60, 68, 70–76, 79, 83–86, 88, 90, 97–99, 152, 164, 180–182, 188–191]. This observation comes with two caveats. First following our recommendation in appendix A, a bird's AR will be lower than in figure 9 as it should be calculated with the total wing area rather than the projected area. Second, most of the reported bird AR's were computed from a fully extended wing due to the difficulty associated with attaining a morphological measurement at the same time as a velocity measurement. In figure 9, the solid data points are true measurements of in-flight projected AR while the hollow circles represent a birds' maximum projected AR and it is known gliding Re or aerodynamic efficiency.

Low Re UAVs often minimize AR for multiple reasons, including controllability, stability and drag concerns [54, 193]. As wing area is maximized to provide controllability and stability, the AR is reduced [64]. Further, increasing the AR of an engineered wing operating at low Re substantially increases the parasitic drag without an equivalent decrease in the vortex-induced drag [193, 194]. Minimizing AR ensures that UAVs will have the largest possible Re to allow any laminar separation to transition and reattach (creating an LSB), which reduces the profile drag on the vehicle and improves its performance compared to fully separated flow conditions [193]. Designing UAVs with these drag constraints in mind allows for low AR designs to provide relatively high aerodynamic efficiency (figure 9(b)).

For small birds, it is possible that higher AR wings are successfully implemented at low Re because the reattachment of LSBs is not a limiting factor in bird flight. Recent bioinspired studies have shown that feather roughness reduces the size of the LSB, thus reducing the form drag and lending credence to this hypothesis [9, 107, 195]. However, one study of artificial owl wings found that feather roughness increased the skin-friction drag causing

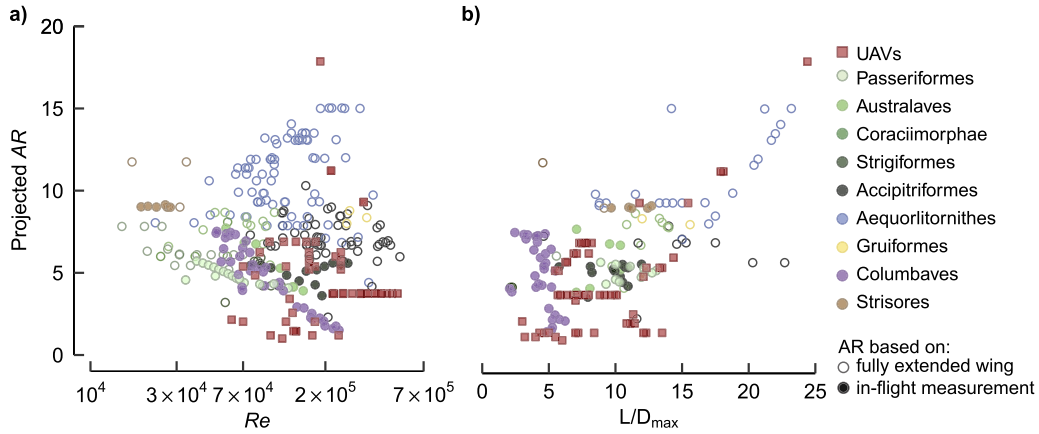

Figure 9. Investigating the effect of projected AR. (a) Projected AR of birds and UAVs as a function of Re. (b) Projected AR of birds and UAVs as a function of $(L/D)_{max}$.

overall performance degradation [195]. This may be a result of varying roughness scales or an owl-specific phenomenon. Feather porosity may also play a role as experiments on porous plates and airfoils (without externally added mass flow) have shown increased skin friction drag compared to smooth models [196–199]. Further investigation of an airfoil with biologically accurate roughness and porosity will be necessary to identify the mechanism that allows birds to effectively utilize high aspect ratios in low Re flows.

We fit a linear model to the aerodynamic efficiency values with explanatory variables of projected AR and Re for the live wind tunnel avian data and the UAV data. This revealed that increasing the projected AR increases the aerodynamic efficiency for both birds and UAVs (avian estimate: 0.61 p-value $=$ 0.04, UAV estimate 0.85: p-value $<$ 0.001). However, when the model was adjusted to include species as an explanatory variable, we found that there were statistically significant differences between common swifts and all other species expect for the western jackdaw (p-value $<$ 0.001). Further, AR no longer had a statistically significant effect (estimate: 0.22 p-value $=$ 0.139). This strong effect of species on the linear model again highlights the importance of avoiding qualitative assumptions of how the AR affects the aerodynamic efficiency especially when comparing across species. This analysis should be enhanced in the future once there are more wind tunnel measurements on live gliding birds to increase the number of observations in the model.

7. Perspectives and future directions

Current challenges in studying avian flight include low Re effects, feather flexibility, roughness, porosity and nonplanarity of the wings. Within this literature survey, we used a single metric $(L/D)_{max}$, to quantify gliding flight performance. $(L/D)_{max}$ is a critical parameter for gliding at low Re due to performance degradation, but this is just one quantifiable gliding flight parameter. Successful gliders must simultaneously optimize other parameters such as endurance, maximum achievable lift coefficient, minimum drag coefficient, and so on [28, 52, 200]. In addition, we focussed only on steady gliding flight rather than soaring flight to allow direct comparisons across species and to UAVs. However, identifying a birds' flight path and analysing the potential benefits and applicability to UAV path planning is an ongoing area of research [82, 97, 98].

The aerodynamic efficiency of a gliding bird has been well studied over the years, but due to the variability of study techniques it has been challenging to extract a clear picture of gliding bird efficiency. To this end, we compiled a complete and comparable dataset of all published gliding bird's aerodynamic efficiency metrics to comment on how efficient birds are relative to similar-sized UAVs and to motivate informed bioinspired UAV designs.

First, we highlighted the uncertainty associated with the theoretical prediction of drag for a gliding bird. We investigated theoretical drag estimates using a component-based decomposition that included vortex-induced drag, profile drag, and parasite drag. Vortex-induced drag for avian wings is currently predicted with Prandtl's lifting line equation for straight, rigid, planar wings, which does not capture the true complexity of avian wings. Cone's equation can predict the minimum vortex-induced drag on a nonplanar rigid wing if its optimum lift distribution is known. Profile and parasite drag coefficients are normally determined from empirically derived constants assumed to be approximately the same for all bird species. Additionally, we found that theoretical avian drag prediction neglects the interference drag between the wing and body, which may substantially affect the overall prediction. Despite the considerable assumptions built into the estimation of each drag component, theoretical drag predictions provide a useful initial estimate for a gliding bird's aerodynamic efficiency. These analytical approaches are especially

valuable when it is not possible to fly a specific species in a controlled environment. Looking forward, the accuracy of theoretical drag predications should be improved by renewed efforts into developing analytical equations for complex wing shapes operating at low Re. To support these theoretical developments, further experimental work using flow imaging technologies like PIV will be required to identify the lift distribution used by a wide variety of species during steady gliding flight.

Next, we investigated and contrasted the different methods used to estimate avian aerodynamic efficiency. We found that glider-based measurements and methods that use theoretical drag predictions to estimate birds' U_s are subject to a high level of uncertainty and large discrepancies between different studies. Radar and rangefinder tracking methods have reduced uncertainty compared to glider-based studies due to their improved ability to satisfy steady glide assumptions throughout a measurement. Wind tunnel measurements further reduce the measurement uncertainty by relocating the bird into a controlled environment. Yet, wind tunnel force measurements on prepared wings and full bird specimens significantly underpredict the expected aerodynamic efficiency of a gliding bird. Given these results, we identified that wind tunnel studies on live gliding birds are the most reliable estimates of a bird's aerodynamic efficiency as they provide a lower bound on the true aerodynamic efficiency. Additionally, wind tunnel studies on live birds can obtain quantitative measures of the wing configurations adopted by a gliding bird at each test condition. Unfortunately, it is not feasible to perform wind tunnel experiments on all species of birds at all flight conditions due to the experimental time and because some birds are too large or too rare to fly in a controlled experimental set up. Therefore, wind tunnel studies are limited to small sample sizes and subject to an individual bird's behaviour.

Are gliding birds more aerodynamically efficiency than modern UAVs? To answer this question, we compared all estimates of avian aerodynamic efficiency to those reported for modern UAVs. Due to the high uncertainty in the theoretical equations and glider-based measurements, we cannot definitively state that birds are more or less efficient than modern UAVs in the supercritical Re regimes. This non-result indicates that advances in experimental and analytical methods are required to reduce the uncertainty in gliding bird aerodynamic efficiency estimates. At that stage, it will be possible to make an informed decision on whether avian inspired UAV designs can yield increased efficiency compared to modern UAV designs in the supercritical Re regimes.

Does the current literature offer any indication about the efficiency of birds vs UAVs in the subcritical Re regimes? Due to the lack of published UAV aerodynamic efficiencies in this range, we hypothesized that the subcritical range is dominated by rotary and flapping-wing UAV designs. As birds use a high projected AR and still efficiently glide in subcritical regimes, future subcritical UAV designs might be able to extend their operational range into lower Re while maintaining high aerodynamic efficiency by drawing inspiration from smaller birds like swifts, jackdaws or falcons. Specifically, future avian inspired UAV designs should focus on identifying which aspect(s) of avian wing morphing will satisfy the mission-specified constraints on geometry, stability and any other applicable categories.

Our survey additionally highlighted two promising questions that could be explored for implementation in avian-inspired UAV design. First, how do species such as pigeons and owls effectively transition from subcritical to supercritical regimes? Second, what are the defining characteristics of the true flow regimes encountered by the rough, porous, flexible avian airfoil?

Extraordinary progress has been made towards understanding gliding bird flight, but more research is required to effectively design future avian-inspired UAVs. Avian flight has inspired many UAV designs; however, it is often accomplished qualitatively rather than quantitatively. It is important to recognize both the progress made by the biological community to quantify aerodynamic parameters of gliding birds and the progress made by the engineering community to design successful low Re UAVs. Contrasting results from both communities has highlighted that it will be necessary to develop improved analytical and experimental methods to predict avian aerodynamic efficiency. These continued efforts will advance a holistic understanding of avian flight and further identify the most beneficial aspects of avian flight that should be used to inform the design of state-of-the-art, highly efficient, low Re UAVs.

8. Conclusions

We provided a summary of published research on avian aerodynamic efficiency in steady gliding flight for the first time, noting the differences in estimation methodologies. This analysis allowed us to identify that theoretical and experimental methods that calculate efficiency with estimates of U_s must be accurate on the order of approximately 0.01 m s^{-1} for differentiable results. Measurements on live birds in controlled environments provide the most reliable minimum estimate of avian gliding efficiency. Next, we provided a survey of the literature on similarly sized, non-copter UAVs. Our comparison between these two groups revealed no evidence that either birds or UAVs operating in supercritical Re regimes are more efficient gliders. However, our survey highlighted the high efficiency of gliding birds in subcritical Re regimes which suggests that future avian-inspired morphing wing UAV designs may be

able to extend their operational capabilities into these lower Re ranges.

Acknowledgments

This work is supported in part by the US Air Force Office of Scientific Research under Grant No. FA9550-16-1-0087, titled 'Avian-inspired multifunctional morphing vehicles' monitored by Dr B L Lee and in part by the National Science Foundation under Grant No.1935216. C Harvey is further supported by a PGS-D though the Natural Sciences and Engineering Research Council of Canada (NSERC) and the Francois-Xavier Bagnoud Fellowship through the University of Michigan Department of Aerospace Engineering. The authors would like to thank V B Baliga, L L Gamble, K P T Haughn and P Sigrest for their helpful insights and discussions on the manuscript.

Appendix A

It is important to recognize that the nondimensional form of Prandtl's solution can be misleading when used for qualitative purposes. Confusion is introduced by the arbitrary selection of the reference area that is used to nondimensionalize the aerodynamic coefficients [115]. For example, the dimensional form of equation (10) reveals that the total induced drag (D_i) is not dependent on a wing's AR or any reference area, but rather on its wingspan as follows:

$$D_i = \frac{L^2}{(1/2)\rho U^2 \pi e_i b^2} \tag{A1}$$

This is especially important to keep in mind when qualitatively comparing wings using AR or a proxy for AR across different species [201, 202]. Consider a hypothetical case of two identical wings except that wing A has a more cambered airfoil than wing B. Focussing only on AR would lead to the conclusion that these wings perform equally. However, wing A will produce more lift and thus have higher vortex-induced drag than wing B. Since there is evidence of a wide variation of airfoil shape between birds species, AR alone should not be used to qualitatively predict trends in vortex-induced drag and thus performance between disparate species [203–205].

Furthermore, the amount of curvature along the wingspan known as spanwise cambering will affect the selected reference area. Currently, it is common practice to use the projected wing area of an extended wing as the reference area in avian flight analyses [110]. However, using the projected wing area causes spanwise cambered bird wings to be nondimensionalized by a reference area that is demonstrably less than their total available lifting surface. Additional challenges arise because the spanwise cambering of a bird's wing varies across its range of motion [165]. This is likely a greater issue for birds with noticeable spanwise cambering such as gulls and with minimal effect for birds with predominately planar wings like swifts. However, we recommend that avian studies use the total wing area to nondimensionalize aerodynamic coefficients and to calculate AR. This captures the total available lifting surface of a bird's wing and facilitates comparisons across varied wing configurations within an individual and across species with different amounts of spanwise cambering.

Appendix B

The Oswald span efficiency factor includes contributions from both vortex-induced drag and the lift-dependent components of parasitic drag [109]. Equation (A2) represents a phenomenological decomposition of drag (figure 4) with the parasitic drag further deconstructed. In the place of $C_{D_{\text{parasitic}}}$ there is a component that is dependent on an empirically-defined relationship with lift ($rC_L{}^2$) and a component that is independent of lift (zero-lift drag, C_{D_0}) as follows:

$$C_D = C_{D_i} + (C_{D_0} + rC_L{}^2) \tag{A2}$$

Regrouping equation (A2) highlights how Prandtl's span efficiency factor (e_i) is related to the Oswald span efficiency factor (e_v) [109, 119]:

$$\begin{aligned} C_D &= C_{D_0} + \left(r + \frac{1}{\pi e_i \mathrm{AR}}\right) C_L{}^2 \\ &= C_{D_0} + \frac{1}{\pi e_v \mathrm{AR}} C_L{}^2 \end{aligned} \tag{A3}$$

ORCID iDs

Christina Harvey https://orcid.org/0000-0002-2830-0844
Daniel J Inman https://orcid.org/0000-0001-6195-1334

References

[1] Baudinette R V and Schmidt-Nielsen K 1974 Energy cost of gliding flight in herring gulls *Nature* **248** 83–4
[2] Tucker V 1972 Metabolism during flight in the laughing gull, Larus atricilla *Am. J. Physiol.* **222** 237–45
[3] Sakamoto K Q, Takahashi A, Iwata T, Yamamoto T, Yamamoto M and Trathan P N 2013 Heart rate and estimated energy expenditure of flapping and gliding in black-browed albatrosses *J. Exp. Biol.* **216** 3175–82
[4] Duriez O, Kato A, Tromp C, Dell'Omo G, Vyssotski A L, Sarrazin F and Ropert-Coudert Y 2014 How cheap is soaring flight in raptors? A preliminary investigation in freely-flying vultures *PloS One* **9** e84887
[5] Sachs G, Traugott J, Nesterova A P, Dell'Omo G, Kümmeth F, Heidrich W, Vyssotski A L and Bonadonna F 2012 Flying at no mechanical energy cost: disclosing the secret of wandering albatrosses *PloS One* **7** e41449
[6] Richardson P L 2011 How do albatrosses fly around the world without flapping their wings? *Prog. Oceanogr.* **88** 46–58

[7] Videler J and Groenewold A 1991 Field measurements of hanging flight aerodynamics in the kestrel Falco tinnunculus *J. Exp. Biol.* **155** 519–30

[8] Abdulrahim M 2004 Dynamic characteristics of morphing micro air vehicles *Masters Dissertation* University of Florida

[9] Di Luca M, Mintchev S, Su Y, Shaw E and Breuer K 2020 A bioinspired separated flow wing provides turbulence resilience and aerodynamic efficiency for miniature drones *Sci. Robot.* **5** eaay8533

[10] Lazos B S 2005 Biologically inspired fixed-wing configuration studies *J. Aircr.* **42** 1089–98

[11] Ákos Z, Nagy M and Vicsek T 2008 Comparing bird and human soaring strategies *Proc. Natl Acad. Sci.* **105** 4139–43

[12] Taylor G K, Reynolds K V and Thomas A L R 2016 Soaring energetics and glide performance in a moving atmosphere *Phil. Trans. R. Soc.* B **371** 20150398

[13] Pennycuick C J 1975 Mechanics of flight *Avian Biology* ed D S Farner and J R King (New York: Academic) pp 1–75

[14] Williamson C J, Spelt A and Windsor S P 2020 Bird-inspired velocity optimization for UAVs in the urban environment *AIAA Scitech 2020 Forum*

[15] Shannon H D, Young G S, Yates M A, Fuller M R and Seegar W S 2002 American white pelican soaring flight times and altitudes relative to changes in thermal depth and intensity *Condor* **104** 679–83

[16] Tennekes H 2009 *The Simple Science of Flight: From Insects to Jumbo Jets* (Cambridge, MA: MIT Press)

[17] Schmitz F W 1967 Aerodynamics of the model airplane. Part 1 – Airfoil measurements report *Technical Memorandum NASA-TM-X-60976* (Redstone Scientific Information Centre) (https://ntrs.nasa.gov/citations/19700029685)

[18] Birch G C, Griffin J C and Erdman M K 2015 *UAS Detection, Classification, and Neutralization: Market Survey 2015* Sandia National Laboratories

[19] Spaar R and Bruderer B 1997 Optimal flight behavior of soaring migrants: a case study of migrating steppe buzzards, Buteo buteo vulpinus *Behav. Ecol.* **8** 288–97

[20] Henningsson P and Hedenström A 2011 Aerodynamics of gliding flight in common swifts *J. Exp. Biol.* **214** 382–93

[21] Ajaj R M, Friswell M I, Bourchak M and Harasani W 2016 Span morphing using the GNATSpar wing *Aerosp. Sci. Technol.* **53** 38–46

[22] Alerstam T, Gudmundsson G A and Larsson B 1993 Flight tracks and speeds of antarctic and atlantic seabirds: radar and optical measurements *Phil. Trans. R. Soc.* B **340** 55–67

[23] Alerstam T 1975 Crane Grus grus migration over sea and land *Ibis* **117** 489–95

[24] Austin R 2011 *Unmanned Aircraft Systems: UAVS Design, Development and Deployment* vol 54 (New York: Wiley)

[25] Bäckman J and Alerstam T 2001 Confronting the winds: orientation and flight behaviour of roosting swifts, Apus apus *Proc. R. Soc.* B **268** 1081–7

[26] Barcala-Montejano M A, Rodríguez-Sevillano A A, Crespo-Moreno J, Bardera-Mora R and Silva-González A J 2015 Optimized performance of a morphing micro air vehicle *2015 Int. Conf. on Unmanned Aircraft Systems (ICUAS)* pp 794–800

[27] Bravo-Mosquera P D, Botero-Bolivar L, Acevedo-Giraldo D and Cerón-Muñoz H D 2017 Aerodynamic design analysis of a UAV for superficial research of volcanic environments *Aerosp. Sci. Technol.* **70** 600–14

[28] Bronz M, Hattenberger G and Moschetta J-M 2013 *Int. J. Micro Air Veh.* **5** 261–72

[29] Bruderer B and Boldt A 2001 Flight characteristics of birds: I. Radar measurements of speeds *Ibis* **143** 178–204

[30] Brusov V S and Petruchik V P 2007 Theoretical and experimental investigations of aerodynamic characteristics for micro-UAV *Proc. 3rd US-European Competition and Workshop on Micro Air Vehicle Systems (MAV07) & European Micro Air Vehicle Conference and Competition (EMAV2007)* pp 17–21

[31] Butler D 2011 *The Design of a Competition Sailplane* SoaringCafe https://soaringcafe.com/2011/01/design-of-a-competition-sailplane/

[32] Demircali A and Uvet H 2018 Mini glider design and implementation with wing-folding mechanism *Appl. Sci.* **8** 1541

[33] Di Luca M, Mintchev S, Heitz G, Noca F and Floreano D 2017 Bioinspired morphing wings for extended flight envelope and roll control of small drones *Interface Focus* **7** 20160092

[34] Durston N E, Wan X, Liu J G and Windsor S P 2019 Avian surface reconstruction in free flight with application to flight stability analysis of a barn owl and peregrine falcon *J. Exp. Biol.* **222** jeb185488

[35] Eder H, Fiedler W and Neuhäuser M 2015 Evaluation of aerodynamic parameters from infrared laser tracking of free-gliding white storks *J. Ornithol.* **156** 667–77

[36] Edwards D 2008 *Performance Testing of RNR's SBXC Using a Piccolo Autopilot* http://www.xcsoaring.com/techPicts/

[37] Edwards D J, Kahn A D, Heinzen S B, Young T Z, Arnold N J, Newton D, Eber B and Carter S V 2018 *CICADA Flying Circuit Board Unmanned Aerial Vehicle 2018 AIAA Aerospace Sciences Meeting*

[38] Grasmeyer J and Keennon M 2001 *Development of the Black Widow Micro Air Vehicle 39th Aerospace Sciences Meeting and Exhibit*

[39] Gruschka H D, Borchers I U and Coble J G 1971 Aerodynamic noise produced by a gliding owl *Nature* **233** 409–11

[40] Gyllhem D, Mohseni K, Lawrence D and Geuzaine P 2005 *Numerical Simulation of Flow Around the Colorado Micro Aerial Vehicle 35th AIAA Fluid Dynamics Conference and Exhibit*

[41] Hacklinger M 1964 Theoretical and experimental investigation of indoor flying models *J. R. Aeronaut. Soc.* **68** 728–34

[42] Hansen T 2014 Modeling the performance of the standard cirrus glider using Navier-Stokes CFD *Tech. Soaring* **38** pp 5–14

[43] Hassanalian M and Abdelkefi A 2017 Design, manufacturing, and flight testing of a fixed wing micro air vehicle with Zimmerman planform *Meccanica* **52** 1265–82

[44] Hassanalian M 2018 *Conceptual Design, Bioinspiration, and Multidisciplinary Analysis of Drones* New Mexico State University Las Cruces, New Mexico, United States of America

[45] Hedenström A 1995 Song flight performance in the skylark Alauda arvensis *J. Avian Biol.* **26** 337–42

[46] Hedenström A and Åkesson S 2017 Adaptive airspeed adjustment and compensation for wind drift in the common swift: differences between day and night *Animal Behav.* **127** 117–23

[47] Hedrick T L, Pichot C and De Margerie E 2018 Gliding for a free lunch: biomechanics of foraging flight in common swifts (Apus apus) *J. Exp. Biol.* **221** jeb186270

[48] Hoey R 2010 Exploring bird aerodynamics using radio-controlled models *Bioinsp. Biomim.* **5** 045008

[49] Horvitz N, Sapir N, Liechti F, Avissar R, Mahrer I and Nathan R 2014 The gliding speed of migrating birds: slow and safe or fast and risky? *Ecol. Lett.* **17** 670–9

[50] Idrac P 1920 *Soaring Flight in Guinea* (Langley Field, VA: National Advisory Committee for Aeronautics Langley Aeronautical Lab)

[51] Jenkins A R 1995 Morphometrics and flight performance of southern African peregrine and lanner falcons *J. Avian Biol.* **26** 49–58

[52] Jin W and Lee Y-G 2014 Computational analysis of the aerodynamic performance of a long-endurance UAV *Int. J. Aeronaut. Space Sci.* **15** 374–82

[53] Junlei S, Zhou Z, Heping W and Shan L 2017 The conceptual design and aerodynamic characteristics analysis of the diamond joined-wing configuration UAV 2017 *5th Int. Conf. on Mechanical, Automotive and Materials Engineering (CMAME) (IEEE)* pp 275–9

[54] Kellogg J *et al* 2001 *The NRL MITE Air Vehicle* (Washington DC: Naval Research Lab)

[55] Kosmatka J 2007 Development of a long-range small UAV for atmospheric monitoring *48th AIAA/ASME/ASCE/AHS/ASC Structures, Structural Dynamics, and Materials Conference*

[56] Kovač M, Zufferey J-C and Floreano D 2009 Towards a self-deploying and gliding robot *Flying Insects and Robots* (Berlin: Springer) pp 271–84

[57] Kroeger R A, Grushka H D and Helvey T C 1972 Wright-Patterson Air Force Base, Ohio Air Force Flight Dynamics Laboratory *Low Speed Aerodynamics for Ultra-Quiet Flight* (Tullhoma, Tennessee: The University of Tennessee Space Institute)

[58] Loftin L K 1985 *Quest for Performance: The Evolution of Modern Aircraft* (Washington, DC: Scientific and Technical Information Branch, National Aeronautics and Space Administration)

[59] Mateos-Rodríguez M and Bruderer B 2012 Flight speeds of migrating seabirds in the Strait of Gibraltar and their relation to wind *J. Ornithol.* **153** 881–9

[60] McGahan J 1973 Gliding flight of the Andean condor in nature *J. Exp. Biol.* **58** 225–37

[61] Meyer S K, Spaar R and Bruderer B 2000 To cross the sea or to follow the coast? Flight directions and behaviour of migrating raptors approaching the mediterranean sea in autumn *Behaviour* **137** 379–99

[62] Meyers R A 1993 Gliding flight in the American kestrel (Falco sparverius): an electromyographic study *J. Morphol.* **215** 213–24

[63] Morgan H L Jr and Paulson J W Jr 1979 *Low-Speed Aerodynamic Performance of a High-Aspect-Ratio Supercritical-Wing Transport Model Equipped with Full-Span Slat and Part-Span Double-Slotted Flaps* (Hampton, VA, United States: NASA Langley Research Center)

[64] Null W and Shkarayev S 2005 Effect of camber on the aerodynamics of adaptive-wing micro air vehicles *J. Aircr.* **42** 1537–42

[65] Panagiotou P, Kaparos P and Yakinthos K 2014 Winglet design and optimization for a MALE UAV using CFD *Aerosp. Sci. Technol.* **39** 190–205

[66] Parrott G C 1970 Aerodynamics of gliding flight of a black vulture Coragyps atratus *J. Exp. Biol.* **53** 363–74

[67] Pennycuick C J 1971 Gliding flight of the white-backed vulture Gyps africanus *J. Exp. Biol.* **55** 13–38

[68] Pennycuick C J 1982 The flight of petrels and albatrosses (procellariiformes), observed in south Georgia and its vicinity *Phil. Trans. R. Soc.* B **300** 75–106

[69] Pennycuick C J 1968 A wind-tunnel study of gliding flight in the pigeon Columba livia *J. Exp. Biol.* **49** 509–26

[70] Pennycuick C J, Alerstam T and Larsson B 1979 Soaring migration of the common crane Grus grus observed by radar and from an aircraft *Ornis Scand.* **10** 241–51

[71] Raspet A 1960 Biophysics of bird flight *Science* **132** 191–200

[72] Rattenborg N C, Voirin B, Cruz S M, Tisdale R, Dell'Omo G, Lipp H-P, Wikelski M and Vyssotski A L 2016 Evidence that birds sleep in mid-flight *Nat. Commun.* **7** 12468

[73] Reynolds K V, Thomas A L R and Taylor G K 2014 Wing tucks are a response to atmospheric turbulence in the soaring flight of the steppe eagle Aquila nipalensis *J. R. Soc. Interface* **11** 20140645

[74] Rosén M and Hedenström A 2002 Soaring flight in the eleonora's falcon (Falco eleonorae) *Auk* **119** 835–40

[75] Rosén M, Spedding G R and Hedenström A 2007 Wake structure and wingbeat kinematics of a house-martin Delichon urbica *J. R. Soc. Interface.* **4** 659–68

[76] Rosen M and Hedenstrom A 2001 Gliding flight in a jackdaw: a wind tunnel study *J. Exp. Biol.* **204** 1153–66

[77] Sampaio R C B, Hernandes A C, Becker M, Catalano F M, Zanini F, Nobrega J L and Martins C 2014 Novel hybrid electric motor glider-quadrotor MAV for in-flight/V-STOL launching *2014 IEEE Aerospace Conf. (IEEE)* pp 1–12

[78] Sarradj E, Fritzsche C and Geyer T 2011 Silent owl flight: bird flyover noise measurements *AIAA J.* **49** 769–79

[79] Shamoun-Baranes J and van Loon E 2006 Energetic influence on gull flight strategy selection *J. Exp. Biol.* **209** 3489–98

[80] Sharma H, Suraj C, Roshan A, Ramesh G, Ahmed S and Narayan P 2013 *Design of a High Altitude Fixed Wing Mini UAV–Aerodynamic Challenges ICIUS 25 Sep 2013 Jaipur*

[81] Shelton A, Tomar A, Prasad J, Smith M J and Komerath N 2006 Active multiple winglets for improved unmanned-aerial-vehicle performance *J. Aircr.* **43** 110–6

[82] Shepard E L C, Williamson C and Windsor S P 2016 Fine-scale flight strategies of gulls in urban airflows indicate risk and reward in city living *Phil. Trans. R. Soc.* B **371** 20150394

[83] Spedding G R 1987 The wake of a kestrel (Falco tinnunculus) in gliding flight *J. Exp. Biol.* **127** 45–57

[84] Spedding G R, Rosén M and Hedenström A 2003 A family of vortex wakes generated by a thrush nightingale in free flight in a wind tunnel over its entire natural range of flight speeds *J. Exp. Biol.* **206** 2313

[85] Tobalske B and Dial K 1996 Flight kinematics of black-billed magpies and pigeons over a wide range of speeds *J. Exp. Biol.* **199** 263–80

[86] Tobalske B and Dial K 1994 Neuromuscular control and kinematics of intermittent flight in budgerigars (Melopsittacus undulatus) *J. Exp. Biol.* **187** 1–18

[87] Tobalske B W 1996 Scaling of muscle composition, wing morphology, and intermittent flight behavior in woodpeckers *Auk* **113** 151–77

[88] Tobalske B 1995 Neuromuscular control and kinematics of intermittent flight in the European starling (Sturnus vulgaris) *J. Exp. Biol.* **198** 1259–73

[89] Tomaszewski A and Goraj Z J 2018 Assessment of a small UAV speed polar graph by conducting flight tests *Aircr. Eng. Aerosp. Technol.* **91** 720

[90] Tucker V A 1987 Gliding birds: the effect of variable wing span *J. Exp. Biol.* **133** 33–58

[91] Tucker V A and Heine C 1990 Aerodynamics of gliding flight in a Harris' hawk Parabuteo unicinctus *J. Exp. Biol.* **149** 469–89

[92] Tucker V A and Parrott G C 1970 Aerodynamics of gliding flight in a falcon and other birds *J. Exp. Biol.* **52** 345–67

[93] Wakeling J and Ellington C P 1997 Dragonfly flight: I. Gliding flight and steady-state aerodynamic forces *J. Exp. Biol.* **200** 543–56

[94] Welch K 1973 Progress in experimental tumor research, vol 17: recent advances in brain tumor research *Arch. Surg.* **106** 612–9

[95] Welch A 1995 Evolution of the high performance glider *Aeronaut. J.* **99** 243–59

[96] White C, Watkins S, Lim E W and Massey K 2012 The soaring potential of a micro air vehicle in an urban environment *Int. J. Micro Air Veh.* **4** 1–13

[97] Williams H J, King A J, Duriez O, Börger L and Shepard E L C 2018 Social eavesdropping allows for a more risky gliding strategy by thermal-soaring birds *J. R. Soc. Interface.* **15** 20180578

[98] Williamson C J, Spelt A and Windsor S P 2020 Bird-inspired velocity optimization for UAVs in the urban environment *AIAA Scitech 2020 Forum*

[99] Wolf T and Konrath R 2015 Avian wing geometry and kinematics of a free-flying barn owl in flapping flight *Exp. Fluids* **56** 28

[100] Biesel W, Butz H and Nachtigall W 1985 Erste Messungen der Flügelgeometrie bei frei gleitfliegenden Haustauben (columbia livia var. domestica) unter Benutzung neu ausgearbeiteter Verfahren der Windkanaltechnik und der Stereophotogrammetrie *Biona-Report* 3 139–60

[101] Anderson J D 1990 *Modern Compressible Flow: With Historical Perspective* vol 2 (New York: McGraw-Hill)

[102] Prum R O, Berv J S, Dornburg A, Field D J, Townsend J P, Lemmon E M and Lemmon A R 2015 A comprehensive phylogeny of birds (Aves) using targeted next-generation DNA sequencing *Nature* **526** 569–73

[103] Alerstam T, Rosén M, Bäckman J, Ericson P G P and Hellgren O 2007 Flight speeds among bird species: allometric and phylogenetic effects *PloS Biol.* **5** e197

[104] Butler P and Woakes A 1980 Heart rate, respiratory frequency and wing beat frequency of free flying barnacle geese Branta leucopsis *J. Exp. Biol.* **85** 213–26

[105] Carmichael B 1981 *Low Reynolds Number Airfoil Survey* vol 1 (Hampton, Virginia: National Aeronautics and Space Administration)

[106] Lissaman P B S 1983 Low-Reynolds-number airfoils *Annu. Rev. Fluid Mech.* **15** 223–39

[107] Lentink D and de Kat R 2014 Gliding swifts attain laminar flow over rough wings *PloS One* **9** e99901

[108] Winslow J, Otsuka H, Govindarajan B and Chopra I 2018 Basic understanding of airfoil characteristics at low Reynolds numbers (104–105) *J. Aircr.* **55** 1050–61

[109] Anderson J D Jr 1989 *Introduction to Flight* (New York: McGraw-Hill)

[110] Pennycuick C J 2008 *Modelling the Flying Bird* vol 5 (Amsterdam: Elsevier)

[111] Anderson J D Jr 2010 *Fundamentals of Aerodynamics* (New York: McGraw-Hill)

[112] Filippone A 2000 Data and performances of selected aircraft and rotorcraft *Prog. Aerosp. Sci.* **36** 629–54

[113] Gur O, Mason W H and Schetz J A 2010 Full-configuration drag estimation *J. Aircr.* **47** 1356–67

[114] Rayner J M V and Maybury W J 2003 The drag paradox: measurements of flight performance and body drag in flying birds *Avian Migration* ed P Berthold, E Gwinner and E Sonnenschein (Berlin: Springer) pp 543–62

[115] Kroo I 2001 Dragdue tolift: concepts for prediction and reduction *Annu. Rev. Fluid Mech.* **33** 587–617

[116] Pennycuick C J 1983 Thermal soaring compared in three dissimilar tropical bird species, Fregata magnificens, Pelecanus occidentals and coragyps atratus *J. Exp. Biol.* **102** 307–25

[117] Rayner J M 1988 Form and function in avian flight *Current Ornithology* (Berlin: Springer) pp 1–66

[118] Prandtl L 1921 *Applications of Modern Hydrodynamics to Aeronautics* National Advisory Committee for Aeronautics

[119] Spedding G R and McArthur J 2010 Span efficiencies of wings at low Reynolds numbers *J. Aircr.* **47** 120–8

[120] Prandtl L 1933 Über tragflügel kleinsten induzierten widerstandes *Z. Flugtechnik Motorluftschiffahrt* **24** 305–6

[121] Hunsaker D F and Phillips W 2020 Ludwig Prandtl's 1933 paper concerning wings for minimum induced drag, translation and commentary *AIAA Scitech 2020 Forum*

[122] KleinHeerenbrink M, Johansson L C and Hedenström A 2017 Multi-cored vortices support function of slotted wing tips of birds in gliding and flapping flight *J. R. Soc. Interface.* **14** 20170099

[123] Tucker V A 1993 Gliding birds: reduction of induced drag by wing tip slots between the primary feathers *J. Exp. Biol.* **180** 285–310

[124] Lynch M, Mandadzhiev B and Wissa A 2018 Bioinspired wingtip devices: a pathway to improve aerodynamic performance during low Reynolds number flight *Bioinspir. Biomim.* **13** 036003

[125] Bachmann T, Blazek S, Erlinghagen T, Baumgartner W and Wagner H 2012 Barn owl flight *Nat. Inspired Fluid Mech.* **119** 101–17

[126] Hassanalian M, Abdelmoula H, Ben Ayed S and Abdelkefi A 2017 Thermal impact of migrating birds' wing color on their flight performance: possibility of new generation of biologically inspired drones *J. Therm. Biol.* **66** 27–32

[127] Rogalla S, D'Alba L, Verdoodt A and Shawkey M D 2019 Hot wings: thermal impacts of wing coloration on surface temperature during bird flight *J. R. Soc. Interface* **16** 20190032

[128] Lee S, Kim J, Park H, Jabłoński P G and Choi H 2015 The function of the alula in avian flight *Sci. Rep.* **5** 9914

[129] KleinHeerenbrink M and Hedenström A 2017 Wake analysis of drag components in gliding flight of a jackdaw (Corvus monedula) during moult *Interface Focus* **7** 20160081

[130] Withers P C 1981 An aerodynamic analysis of bird wings as fixed aerofoils *J. Exp. Biol.* **90** 143–62

[131] Tucker V A 1998 Gliding flight: speed and acceleration of ideal falcons during diving and pull out *J. Exp. Biol.* **201** 403–14

[132] Cone C D Jr 1962 *The Theory of Induced Lift and Minimum Induced Drag of Nonplanar Lifting Systems* National Aeronautics and Space Administration Springfield, VA, United States of America

[133] Cone C D Jr 1963 *The Aerodynamic Design of Wings with Cambered Span Having Minimum Induced Drag* National Aeronautics and Space Administration Langley Research Center Hampton, VA, United States of America

[134] Tucker V A 1995 Drag reduction by wing tip slots in a gliding Harris' hawk, Parabuteo unicinctus *J. Exp. Biol.* **198** 775–81

[135] Ranjan P, Ansell P J and James K A 2019 Optimal hyperelliptic cambered span configurations for minimum drag *J. Aircr.* **56** 356–68

[136] Lazos B and Visser K 2006 Aerodynamic comparison of hyper-elliptic cambered span (HECS) wings with conventional configurations *24th AIAA Applied Aerodynamics Conf. Fluid Dynamics and Co-located Conferences* (American Institute of Aeronautics and Astronautics) pp 1–18

[137] Usherwood J R, Hedrick T L and Biewener A A 2003 The aerodynamics of avian take-off from direct pressure measurements in Canada geese (Branta canadensis) *J. Exp. Biol.* **206** 4051–6

[138] Usherwood J R, Cheney J A, Song J, Windsor S P, Stevenson J P J, Dierksheide U, Nila A and Bomphrey R J 2020 High aerodynamic lift from the tail reduces drag in gliding raptors *J. Exp. Biol.* **223** jeb214809

[139] Bowers A H, Murillo O J, Jensen R R, Eslinger B and Gelzer C 2016 *On Wings of the Minimum Induced Drag: Spanload Implications for Aircraft and Birds* National Aeronautics and Space Administration Armstrong Flight Research Center Edwards, California, United States of America

[140] Phillips W F, Hunsaker D F and Joo J J 2019 Minimizing induced drag with lift distribution and wingspan *J. Aircr.* **56** 431–41

[141] Taylor G and Thomas A 2014 *Evolutionary Biomechanics* (Oxford: Oxford University Press)

[142] Lundry J L and Llssaman P B S 1968 A numerical solution for the minimum induced drag of nonplanar wings *J. Aircr.* **5** 17–21

[143] Pennycuick C, Heine C E, Kirkpatrick S J and Fuller M R 1992 The profile drag of a hawk's wing, measured by wake sampling in a wind tunnel *J. Exp. Biol.* **165** 1–19

[144] Dabiri J O 2005 On the estimation of swimming and flying forces from wake measurements *J. Exp. Biol.* **208** 3519–32

[145] Hazan O 2012 *Turbulent Flow Characterization and Aerodynamic Forces Around a Gliding Osprey Model in a*

Wind Tunnel (Beersheba, Israel: Ben-Gurion University of the Negev)
[146] KleinHeerenbrink M, Warfvinge K and Hedenström A 2016 Wake analysis of aerodynamic components for the glide envelope of a jackdaw (Corvus monedula) *J. Exp. Biol.* **219** 1572
[147] Pennycuick C, Obrecht H H and Fuller M R 1988 Empirical estimates of body drag of large waterfowl and raptors *J. Exp. Biol.* **135** 253–64
[148] Pennycuick C, Klaassen M, Kvist A and Lindström Å 1996 Wingbeat frequency and the body drag anomaly: wind-tunnel observations on a thrush nightingale (Luscinia luscinia) and a teal (Anas crecca) *J. Exp. Biol.* **199** 2757–65
[149] Pennycuick C J 1969 The mechanics of bird migration *Ibis* **111** 525–56
[150] Hedenstrom A and Liechti F 2001 Field estimates of body drag coefficient on the basis of dives in passerine birds *J. Exp. Biol.* **204** 1167–75
[151] Maybury W J 2000 *The Aerodynamics of Bird Bodies* University of Bristol Bristol
[152] Nachtigall W 1998 Starlings and starling models in wind tunnels *J. Avian Biol.* **29** 478–84
[153] Tucker V A 2000 Gliding flight: drag and torque of a hawk and a falcon with straight and turned heads, and a lower value for the parasite drag coefficient *J. Exp. Biol.* **203** 3733–44
[154] Tucker V A 1990 Body drag, feather drag and interference drag of the mounting strut in a peregrine falcon, Falco peregrinus *J. Exp. Biol.* **149** 449–68
[155] Pennycuick C J, Åkesson S and Hedenström A 2013 Air speeds of migrating birds observed by ornithodolite and compared with predictions from flight theory *J. R. Soc. Interface* **10** 20130419
[156] Nudds R L and Rayner J M V 2006 Scaling of body frontal area and body width in birds *J. Morphol.* **267** 341–6
[157] Delany N K and Sorensen N E 1953 *Low-Speed Drag of Cylinders of Various Shapes* (Ames Aeronautical Laboratory: National Advisory Committee for Aeronautics) Washington, DC, United States of America
[158] Judd M, Vlajinac M and Covert E E 1971 Sting-free drag measurements on ellipsoidal cylinders at transition Reynolds numbers *J. Fluid Mech.* **48** 353–64
[159] Maybury W J and Rayner J M V 2001 The avian tail reduces body parasite drag by controlling flow separation and vortex shedding *Proc. R. Soc.* B **268** 1405–10
[160] Johansson L C and Hedenström A 2009 The vortex wake of blackcaps (Sylvia atricapilla L.) measured using high-speed digital particle image velocimetry (DPIV) *J. Exp. Biol.* **212** 3365–76
[161] Spear L B and Ainley D G 1997 Flight behaviour of seabirds in relation to wind direction and wing morphology *Ibis* **139** 221–33
[162] Alerstam T 1987 Radar observations of the stoop of the peregrine falcon Falco peregrinus and the goshawk Accipiter gentilis *Ibis* **129** 267–73
[163] Azuma A 1992 Flight by gliding *The Biokinetics of Flying and Swimming* (Berlin: Springer) pp 19–75
[164] Pennycuick C 1960 Gliding flight of the fulmar petrel *J. Exp. Biol.* **37** 330–8
[165] Harvey C, Baliga V B, Lavoie P and Altshuler D L 2019 Wing morphing allows gulls to modulate static pitch stability during gliding *J. R. Soc. Interface* **16** 20180641
[166] Reddig E 1978 Der ausdrucksflug der Bekassine (Capella gallinago gallinago) *J. Ornithol.* **119** 357–87
[167] Lentink D *et al* 2007 How swifts control their glide performance with morphing wings *Nature* **446** 1082
[168] Klaassen van Oorschot B, Mistick E A and Tobalske B W 2016 Aerodynamic consequences of wing morphing during emulated take-off and gliding in birds *J. Exp. Biol.* **219** 3146–54
[169] Lees J J, Dimitriadis G and Nudds R L 2016 The influence of flight style on the aerodynamic properties of avian wings as fixed lifting surfaces *Peer J.* **4** e2495
[170] Pennycuick C J 1982 The ornithodolite: an instrument for collecting large samples of bird speed measurements *Phil. Trans. R. Soc.* B **300** 61–73
[171] Safran Vectronix *AG VECTOR FAMILY Rangefinder Binoculars* https://www.safran-vectronix.com/
[172] Henningsson P, Spedding G R and Hedenström A 2011 Vortex wake and flight kinematics of a swift in cruising flight in a wind tunnel *J. Exp. Biol.* **214** 697
[173] Gillies J A, Thomas A L R and Taylor G K 2011 Soaring and manoeuvring flight of a steppe eagle Aquila nipalensis *J. Avian Biol.* **42** 377–86
[174] Williams H, Shepard E, Duriez O and Lambertucci S A 2015 Can accelerometry be used to distinguish between flight types in soaring birds? *Animal Biotelem.* **3** 45
[175] Lian Y and Shyy W 2007 Laminar-turbulent transition of a low Reynolds number rigid or flexible airfoil *AIAA J.* **45** 1501–13
[176] Loxton B 2011 *An Experimental Investigation into the Effects of Atmospheric Turbulence on the Aerodynamics of Micro Air Vehicle Wings* RMIT University Melbourne, Australia
[177] Bomphrey R J 2012 Advances in animal flight aerodynamics through flow measurement *Evol. Biol.* **39** 1–11
[178] Deetjen M E, Chin D D and Lentink D 2020 The aerodynamic force platform as an ergometer *J. Exp. Biol.* **223** 220475
[179] Henningsson P, Hedenström A and Bomphrey R J 2014 Efficiency of lift production in flapping and gliding flight of swifts *PloS One* **9** e90170
[180] Le Page W L 1923 Wind channel experiments on a pariah kite *J. R. Aeronaut. Soc.* **27** 114–5
[181] Feldmann E 1944 *Windkanaluntersuchungen am modell einer möwe Luftfahrttechnik* **19** 219–22
[182] Nayler J and Simmons L 1920 *A Note Relating to Experiments in a Wind Channel with an Alsatian Swift* (HM Stationery Office) Great Britain
[183] Pelletier A and Mueller T J 2000 Low Reynolds number aerodynamics of low-aspect-ratio, thin/flat/cambered-plate wings *J. Aircr.* **37** 825–32
[184] Elston J, Argrow B, Stachura M, Weibel D, Lawrence D and Pope D 2015 Overview of small fixed-wing unmanned aircraft for meteorological sampling *J. Atmos. Ocean. Technol.* **32** 97–115
[185] Deperrois A 2019 *Theoretical Limitations and Shortcomings of xflr5* http://www.xflr5.tech/docs/Part%20IV:%20Limitations.pdf
[186] Najm H N 2009 Uncertainty quantification and polynomial chaos techniques in computational fluid dynamics *Annu. Rev. Fluid Mech.* **41** 35–52
[187] Oberkampf W L and Blottner F G 1998 Issues in computational fluid dynamics code verification and validation *AIAA J.* **36** 687–95
[188] Thomas A L R and Taylor G K 2001 Animal flight dynamics: I. Stability in gliding flight *J. Theor. Biol.* **212** 399–424
[189] Bernstein M H, Thomas S P and Schmidt K 1973 Power input during flight of the fish crow, Corvus ossifragus *J. Exp. Biol.* **58** 401–10
[190] Henningsson P, Karlsson H, Bäckman J, Alerstam T and Hedenström A 2009 Flight speeds of swifts (Apus apus): seasonal differences smaller than expected *Proc. R. Soc.* B **276** 2395–401
[191] McLaren J D, Shamoun-Baranes J, Camphuysen C J and Bouten W 2016 Directed flight and optimal airspeeds: homeward-bound gulls react flexibly to wind yet fly slower than predicted *J. Avian Biol.* **47** 476–90
[192] Richardson P L, Wakefield E D and Phillips R A 2018 Flight speed and performance of the wandering albatross with respect to wind *Mov. Ecol.* **6** 3

[193] Shkarayev S V, Ifju P G, Kellogg J C and Mueller T J 2007 *Introduction to the Design of Fixed-Wing Micro Air Vehicles Including Three Case Studies* (Reston, VA,: American Institute of Aeronautics and Astronautics) https://doi.org/10.2514/4.862106
[194] Bramesfeld G 2010 Small and micro aerial vehicles: how much span is too much span? *J. Aircr.* **47** 1982–90
[195] Winzen A, Klaas M and Schröder W 2014 High-speed particle image velocimetry and force measurements of bio-inspired surfaces *J. Aircr.* **52** 471–85
[196] Wilkinson S 1983 Influence of wall permeability on turbulent boundary-layer properties *21st Aerospace Sciences Meeting*
[197] Geyer T, Sarradj E and Fritzsche C 2010 Measurement of the noise generation at the trailing edge of porous airfoils *Exp. Fluids* **48** 291–308
[198] Geyer T F and Sarradj E 2019 Self Noise Reduction and Aerodynamics of Airfoils with Porous Trailing Edges *Acoustics* **1** 393–409
[199] Hajian R and Jaworski J W 2017 The steady aerodynamics of aerofoils with porosity gradients *Proc. R. Soc.* A **473** 20170266
[200] Poh C-K and Poh C-H 2015 UAV with VTOL and endurance capability inspired by unlimited-class aerobatic aircraft *Int. J. Micro Air Veh.* **7** 125–32
[201] Sheard C, Neate-Clegg M H, Alioravainen N, Jones S E, Vincent C, MacGregor H E, Bregman T P, Claramunt S and Tobias J A 2020 Ecological drivers of global gradients in avian dispersal inferred from wing morphology *Nature Commun.* **11** 1–9
[202] Kennedy J D, Borregaard M K, Jønsson K A, Marki P Z, Fjeldså J and Rahbek C 2016 The influence of wing morphology upon the dispersal, geographical distributions and diversification of the Corvides (Aves; Passeriformes) *Proc. R. Soc. B.* **283** 20161922
[203] Aono H, Kondo K, Nonomura T, Anyoji M, Oyama A, Fujii K and Yamamoto M 2020 Aerodynamics of owl-like wing model at low Reynolds numbers *Trans. Japan Soc. Aeronaut. Space Sci.* **63** 8–17
[204] Liu T, Kuykendoll K, Rhew R and Jones S 2006 Avian wing geometry and kinematics *AIAA J.* **44** 954–63
[205] Ananda G K and Selig M S 2018 Design of bird-like airfoils *2018 AIAA Aerospace Sciences Meeting* p 0310